UNIVERSITY OF OKLAHOMA

GRADUATE COLLEGE

CALCULATION OF ESTIMATED OIL RECOVERY USING CARTER TYPE CURVES

A THESIS

SUBMITTED TO THE GRADUATE FACULTY

in partial fulfillment of the requirements for the

Degree of

MASTER OF SCIENCE

By

NOSIRAT AJOKE GOODLUCK
Norman, Oklahoma
2017

CALCULATION OF ESTIMATED OIL RECOVERY USING CARTER TYPE CURVES

A THESIS APPROVED FOR THE
MEWBOURNE SCHOOL OF PETROLEUM AND GEOLOGICAL ENGINEERING

BY

Dr. Deepak Devegowda, Chair

Dr. Faruk Civan

Dr. Chandra Rai

Dr. Mashhad Fahs

I would like to dedicate this thesis to my parents, Dr. and Hon. (Mrs.) Goodluck, and my grandmother Alhaja Kuburat Alli-Balogun and my aunt Mrs. Johnson for your investments in me. My sister Jade and Lolu Goodluck for encouraging me.

To my great granfather, Alli Balogun of Lagos, grandfather Comrade Wahab Omorilewa Goodluck and Comrade Aka-Bashorun your contributions to our society has kept me focused and determined, and be worthy of your name.

“**A thousand ants can never kill a Lion**”

An African proverb that has strengthened me at all times.

Acknowledgements

I would like to thank to my God Almighty and his son Jesus Christ for standing by me day and night. I thank my advisor, Dr. Rai for his dedication and Prof. Fahs for her devotion to success. I thank Dr. Civan for being the person who made me choose Reservoir Engineering as a career and joining the Shale Gas Reservoir Consortium, at the beginning of my research he laid the foundations that I use until today. To a few friends in Tunde Osholanke and Obinna Duru thank you for the support.

Table of Contents

List of Tables

List of Figures

Abstract

The focus of this research is to calculate the Estimated Ultimate Recovery (EUR) of shale wells for a diverse range of fluid types using Carter (1985) type curves. The Carter (1985) type curve is a plot of flow rate versus time in dimensionless form and originally developed for dry gas and under-saturated black oil reservoirs. One of the key advantages of the Carter (1985) type curves is that it accounts for different flow regimes such as transient, infinite-acting flow and boundary-dominated flow as well as fluid properties such as viscosity and compressibility. However, because it relies on the use of well-defined and pressure-sensitive fluid properties such as viscosity and compressibility, the Carter (1985) type curves cannot easily generalized to multiphase flow or flow of more complex fluid types.

In this thesis, I extend the use of Carter (1985) type curves to wet gas, gas-condensate and volatile oil reservoirs for flow above and below their respective saturation pressures. This is achieved by determining an effective viscosity-compressibility product that can be used in the Carter (1985) type curves. This viscosity-compressibility product is then correlated against fluid C_{7+} fractions so that the practicing reservoir engineer can easily look-up the appropriate viscosity-compressibility product values for use in EUR calculations using Carter (1985) type curves.

Chapter One: Introduction

This chapter provides an overview of the Carter (1985) type curve method, its mathematical formulation and application. I also present a discussion of other decline curve and type curve methods and illustrate the advantages of the Carter (1985) type curve approach.

1.1 Carter Type Curve Equations

Carter (1985) numerically generated type curves tailored for gas rate-time analysis using a depletion parameter, λ to quantify the impact of pressure drawdown and the viscosity and compressibility product, $\mu_g c_g$. The type curves replicated in this research are derived from Carter (1985) developed for real gases in a linear flow regime. The decline curve analysis for a constant-pressure boundary is to predict depleting flowrates that is first mathematically expressed by Moore, Schilthius and Hurst (1933). This is applied by Fetkovich (1980) for infinite and finite, slightly compressible, single-phase radial flow system using dimensionless flow rate, q_D and dimensionless time, t_D as defined in equations 1 and 2:

$$q_D = \frac{141.3 q_{(t)} \mu B}{kh(p_i - p_{wf})} \qquad (1)$$

$$t_D = \frac{0.00634 kt}{\phi \mu c r_w{}^2} \qquad (2)$$

Where B is the formation volume factor, q(t) is the flow rate at a specific time, μis the viscosity, p_i is the initial pressure, p_{wf} is the bottom hole flowing pressure, k is the permeability, h is the thickness, Φ is the porosity, c is the compressibility and r_w is the internal radius. Carter (1981) proposed an empirical correlation for the pseudo production rate and pseudo time for gas wells from the diffusivity equation using instantaneous values of pressure dependent properties sourced from Al-Hussainy, Ramey and Crawford (1966). The major parameter, b for the Arps (1945) decline curves. λ depends on $\mu_g c_g$ when the reservoir starts depleting and enters boundary dominated flow. Carter (1985) equations assumes the fluid is either a gas with $\mu_g c_g$ varying with pressure or oil with constant $\mu_o c_o$. A few additional parameters include the fraction of the radial flow region, σ, and the time co-efficient, α_j. Carter (1981) equations for dimensionless rate is:

$$q_D = \frac{1424 \mathrm{qT}(\frac{1}{\mathrm{B_1}})}{\sigma \mathrm{kh}[\, m(p_i) - m(p_{wf})]} \tag{3}$$

Where q is flow rate, T is temperature, B_1 is the first-order coefficient derived from series expansion of dimensionless flow rate in terms of first-order Bessel functions. m (p_i) is the real gas pseudo pressure of real gas flow potential at initial pressure, m(p_{wf}) is the real gas pseudo pressure of real gas flow potential at bottom hole flowing pressure, k is permeability and h is the reservoir thickness (Lee and Wattenbarger 1996, 228-229).

And dimensionless time is:

$$t_D = \frac{2.634 \mathrm{x} 10^{-4} \mathrm{x} 24 \mathrm{kt} \alpha_1}{\phi \mu(p_i) c_g(p_i) {r_w}^2} \tag{4}$$

Where k is the permeability, t is time in days, α_1 is the first-order coefficient derived from series expansion of dimensionless flow rate in terms of first-order Bessel functions, Φ is the porosity, μ is the viscosity, c_g is the gas compressibility, r_w is the internal radius of type curve reservoir region (Lee and Wattenbarger 1996, 228-229).

The reservoir flow geometry parameter dominating the transient phase period;

$$\eta = \frac{(R^2-1)}{2}\left(\frac{\alpha_1^2}{B_1}\right) \quad (5)$$

Where R=r_e/r_w which is the ratio of r_e that is the drainage radius and r_w the wellbore radius.

$$\lambda = \frac{\mu(p_i)c_g(p_i)}{2} x \frac{[m(p_i)-m(p_{wf})]}{[\left(\frac{p}{z}\right)i-\left(\frac{p}{z}\right)wf]} \quad (6)$$

The equations are used in creating Figure 1.1 for radial-linear gas reservoir type curves. The curves in the transient flow regime represent different values of η and the three curves during boundary-dominated flow (BDF) represent different values of λ.

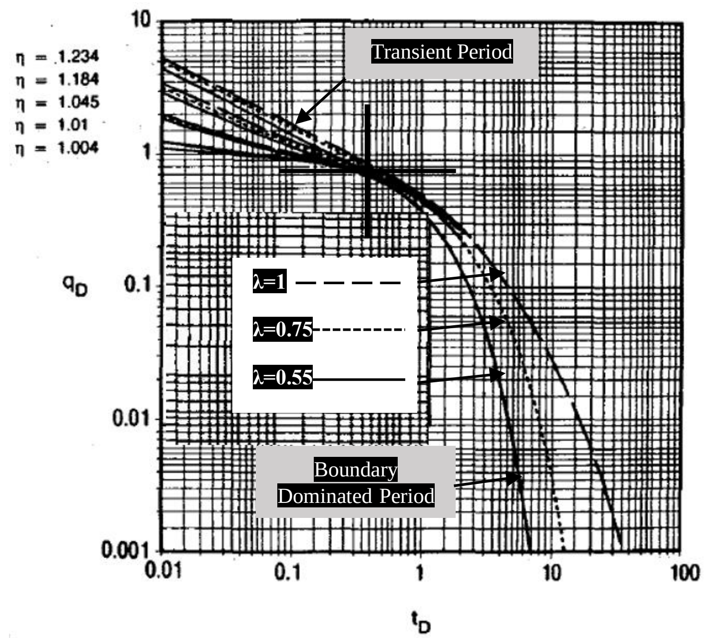

Figure 1.1– Radial-linear gas-reservoir type curves (Carter 1985). The transient and boundary period separated with the demarcation. The three bottom concave curves are for λ=0.55, 0.75 and 1 from left to right.

The flow geometry concept η, introduced by Carter (1981) uses the α_1 is the j_{th} root and B_1 is the coefficient of the j_{th} transforms which model radial-linear flow systems for exact liquid (λ=1) flow solution for cumulative production as a function of time for radial system. It's used in obtaining the exact solution for production rate as a function of time.

Carslaw and Jagger (1940) introduced the concept of $\alpha_{1,}$ is the time co-efficient which is the root of the Bessel functions and B_j is the coefficient of the modified Bessel functions of the first and second kind of arguments.

1.2 Mathematical Modeling of Carter Dimensionless Rate and Time Equations

The constant terminal pressure and constant terminal rate solutions by Everdingen and Hurst (1949) to model aquifer influx forms the basis of the Carter (1981) curves. Carter (1985) adapted the constant terminal pressure solution proposed by Carslaw and Jaeger (1941), van Everdingen, and Hurst (1949) to estimate production rate as a function of time as shown in Equation 8 below:

$$q_{\mathrm{DR}}(t_{DR}) = \sum_{j=1}^{\infty} \mathrm{B_j} e^{-\alpha_j^2 * t_{DR}} \tag{8}$$

where $$\mathrm{B_j} = \frac{2\, J_1^2(\alpha_j \mathrm{R})}{[\, J_0^2(\alpha_j) - J_1^2(\alpha_j R)\,]} \tag{9}$$

and α_j is the jth root of

$$J_1(\alpha_j R)\, Y_o(\alpha_j) - Y_1(\alpha_j R)\, J_o(\alpha_j) = 0 \tag{10}$$

Where q_{DR} and t_{DR} are dimensionless rate and time for radial-linear flow used in the J_1 and J_o is the Bessel function of the first kind of order 1 and 0 respectively and Y_1 and Y_o Bessel function of the second kind of order 1 and 0 used by van Everdingen, and Hurst (1949) based on Carslaw and Jaeger (1941). This equation is used in a mathematical code that estimated α_j for 50 roots used to calculate the Bessel function B_1 to B_j used in equations 6,7 and 8. The range of 0.001 to 4.2 was used as values of $t_{D,}$ and q_D was calculated with the Equation 11:

$$q_D = e^{-t_D} + \sum_{j=1}^{\infty} \frac{B_J}{B_1} e^{-(\alpha_j^2/\alpha_1^2) t_D} \quad (11)$$

The graphical results using this equation above for R=10 is displayed in Fig. 1.2.

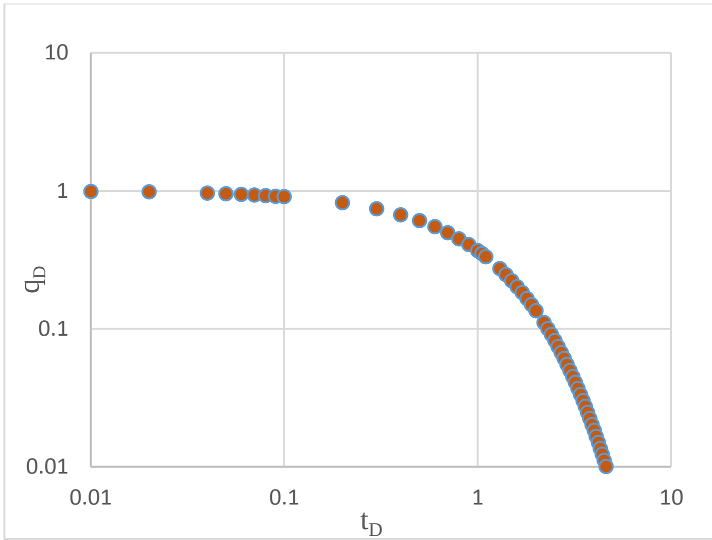

Figure 1.2— Calculated q_D vs t_D type curves replicating the original λ=0.55 type curves using R=10 (after Carter 1985).

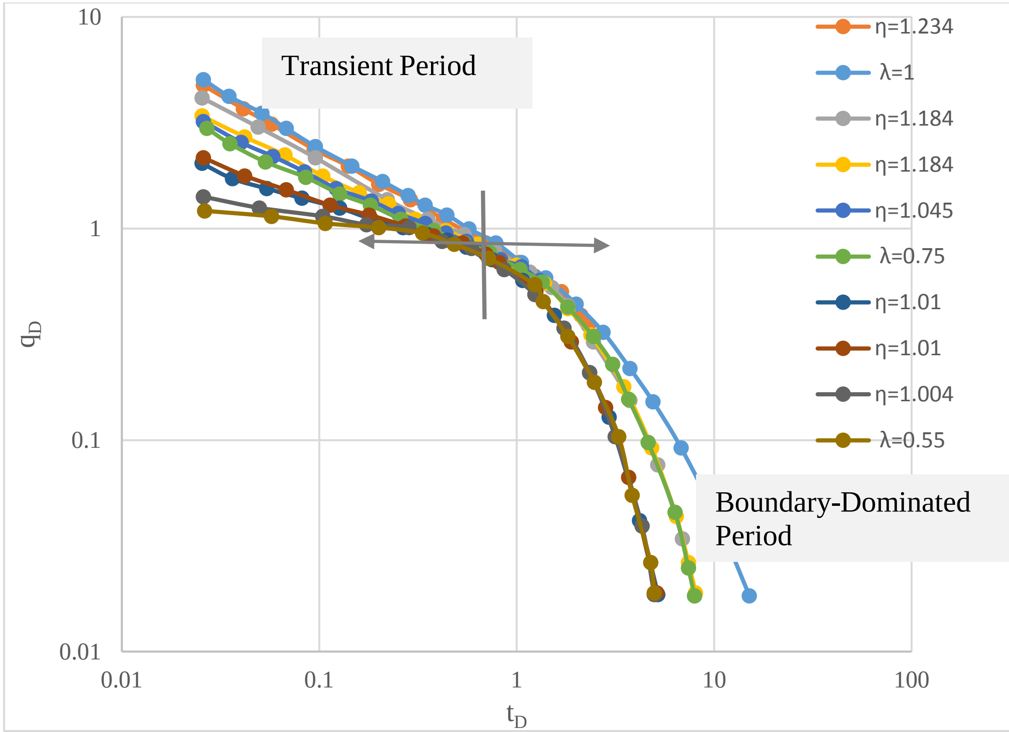

Figure 1.3— Digitized Carter's type curve (after Carter 1985). The transient period is separated from the boundary period with the cross arrows.

1.3 Application of Carter Type Curves

The rate time behavior of gas reservoirs producing with constant terminal pressure is governed by the reservoir boundaries and fluid properties during boundary dominated flow (Carter 1981). Arps (1945) equation has always been considered to be "purely empirical with no basis in physical laws governing the flow of oil and gas" (Fetkovich et al. 1987). Ayala and Ye (2012) extensively used Carter (1985) work extensively to obtain a density-based variable that is a modification of $\mu_g c_g$ ratio. Their density methodology is a rigorous and has been validated analytically with several field and numerical cases. Fetkovich (1987) also used Carter (1985) type curve in their analysis of the West Virginia well that had produced for eight years, this case study incorporated Arps (1945) application to determine the gas in place at different drawdown pressures. The results obtained using b=0 and b=0.5 was validated using Carter (1985) type curve match at λ=0.55 to show that the gas in place calculated at b=0.5 must be used because of the close values obtained from Carter (1985) type curve match.

1.4 Literature Review of EUR Calculations

There are alternative techniques to EUR calculations besides decline curve analysis (DCA) such as the classical volumetric, material balance or production history matching used by reservoir engineers. These methods can calculate the amount of oil and gas in place, but to establish the actual EUR requires the use of simulations that accounts for oil and gas that is cannot be recovered. These methods may require access to data that may not be readily available, such as the geological model, reservoir simulation tools, PVT data and core/well-log data. In practice, decline curve analysis may be more appropriate than the conventional volumetric or material-balance methods because of a lack of data for adequate reservoir description.

1.4.1 Decline Curves

The type curves are "theoretical solutions to flow equations" that can be used for all types of reservoir models with different flow regimes. All decline analysis use type curves that have assumptions behind the solutions (Lee and Wattenbarger 1996, 219). These is further discussed for Fetkovich (1980) and Carter (1985). In this thesis a focus on the theoretical and practical applications that make them extremely useful in gas wells decline analysis. The two type curves both do not consider non-Darcy effects and are based on theoretical considerations unlike Arps (1945) which uses empirical decline curve analysis techniques. A unique advantage of decline curves is that it allows us to estimate not "only the original gas in place and gas reserves at the abandonment conditions but it estimates the flowing characteristic of individual" (Lee and Wattenbarger 1996, 219 -220). This is a major difference between volumetric and material balance equations with decline curves, hence the use of information of the flow characteristics gives precisely the estimated ultimate recovery that is the recoverable volume of oil and gas.

An example of a decline curve used to calculate EUR is by Rodrigues and Callard (2012). "They used a modified plot of cumulative production vs the square root of produced time in estimating the end of linear flow while modeling the cumulative oil and gas produced". In their example an Eagle ford shale well is modeled to estimate the end of linear flow and the start of boundary dominated flow.

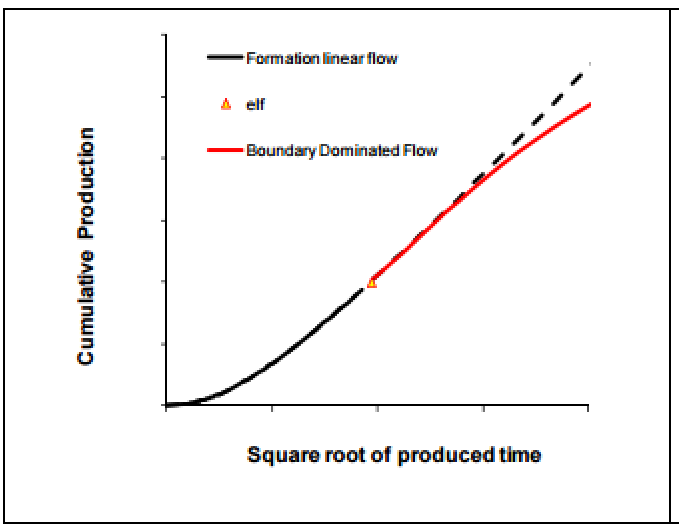

Figure 1.4— Cumulative Production vs square root of produced time for finite conductivity fractures (after Rodrigues and Callard 2012).

1.4.2 Reservoir Simulation

The industry has several software's that can calculate EUR like the Monte Carlo or DCA software packages that Arps (1945) equation after the production data has given a b, decline curve exponent value. The use of reservoir simulation is a viable method for solving problems such as gases, with non-linearity of equations has become a reliable method for solving reservoir flow problems in offices and laboratories. The pitfall of the simulator for calculating the EUR is that it requires information that is not always available or economically possible for some companies such as well logs, core analysis, geological description, pressure data, production data and laboratory analysis. If the wells have produced the past production period is simulated for history matching where input data must be adjusted to match past performance through a calibration process to give an accurate reservoir model for future forecasts. There is an alternative to analytical solutions which is the finite difference approach which is popularly known as reservoir simulation (Lee and Wattenbarger,1996). Some modern approaches to using reservoir simulation to calculate EUR is seen in Swami et al (2017) where multiple simulations are used in many diagnostic plots to calculate the EUR. The recovery factor is determined after history match of 580 days and 30 years, which is applied to the simulated EUR, obtained from the cumulative production vs time plot.

Monifar et al. (2016) did a critical review of the wells EUR when using analytical model-based rate-transient-analysis, RTA vs the numerical simulation-based workflow in low permeability wells. Monifar et al. (2016) focused on the impact of using analytical solution-based methods for multiphase flow. The overall results showed that the numerical solution model using the cumulative oil forecast generated using the simulation P50 model gave an excellent agreement with the finely-gridded reference solution while the cumulative oil forecast generated using RTA history match model underestimated the oil EUR. Henceforth, the use of numerical simulations is ideal for EUR calculations.

1.5 Methods for Production Data Analysis

In this section I discuss the various commonly employed methods for production data analysis and discuss some of their drawbacks in addressing the needs unique to complex fluids such as gas condensates and volatile oil reservoirs.

1.5.1 Traditional Decline Curves

The first attempts for DCA is aimed at graphical methods or functions that could linearize production data. The analysis of a linear graph is easy to understand and change it mathematically and graphically so that the results are extended to forecast of the future production forecast if it is assumed that the linear trend continued for the life of the well. “The most common conventional DCA technique plotted is on a linear semi log known as exponential or constant-percentage decline” (Lee and Wattenbarger 1996, 214-215) . Arps (1945) “is accounted as the first to use this ideology, his work proved that not all wells can be modeled with the exponential decline and recognized that some wells could also be harmonic or hyperbolic because they may not fit an exponential decline” (Lee and Wattenbarger 1996, 214-215). Henceforth, most conventional DCA used in the industry based on Arps (1945) empirical rate/time decline presented in Equation 18, which has been used by other DCA authors.

$$q_{(t)} = \frac{q_i}{(1+bD_i t)^{1/b}} \tag{18}$$

$$D_i = -dq(t)/dt/q(t) \tag{19}$$

D_i will represent the initial decline rate in days^{-1} and b is the decline curve exponent.

The different decline exponent b, has three different values for exponential, harmonic and hyperbolic declines. This equation assumes a “constant BHP, unchanged drainage area with no flow boundaries, constant permeability and skin factor and is applicable only to boundary dominated flow regimes" (Lee and Wattenbarger 1996, 214-215).

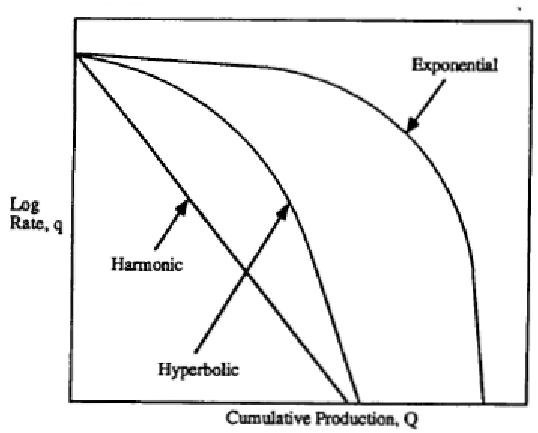

Figure 1.5: Decline curve shapes for semi log plot of rate vs cumulative production (Lee and Wattenbarger 1996).

1.5.2 Exponential Decline

Lee and Wattenbarger (1996) defined this as "the constant-percentage decline; it is characterized by a decrease in production rate per unit of time that is proportional to the production rate". Therefore, b=0.

$$q(t) = \frac{q_i}{e^{D_i t}} = q_i e^{-D_i t} \tag{20}$$

Equation 20 after re-arrangement becomes:

$$log[q(t)] = \log(q_i) - \frac{D_i t}{2.303} \tag{21a}$$

The cumulative production G_p is given by:

$$G_p(t) = \frac{1}{D_i} q(t) + \frac{q_i}{D_i} \tag{21b}$$

1.5.3 Harmonic Decline

This is when b=1, so the decline curve equation becomes:

$$q(t) = \frac{q_i}{(1+D_i t)} \tag{23}$$

$$log[q(t)] = log(q_i) - log(1 + D_i t) \tag{24}$$

The equation above shows "that q(t) is a linear function of (1+D_it) on log-log graph paper and will exhibit a straight line with a slope of -1 and an intercept of log q_i" (Lee and Wattenbarger 1996, 216-217).

1.5.4 Hyperbolic Decline

When 0 <b<1 the decline is hyperbolic and the rate behavior is defined as:

$$q(t) = \frac{q_i}{(1+bD_i t)^{1/b}} \tag{27}$$

$$log[q(t)] = log(q_i) - \frac{1}{b} log(1 + bD_i t) \tag{28}$$

The slope of the hyperbolic decline 1/b will have an intercept of log (q_i) when the plot of log [q(t)] vs. log (1+bD_it) exhibits a straight line (Lee and Wattenbarger 1996, 216-217).

1.6 Fetkovich Rate Time Type Curve Analysis

The work of Fetkovich et al. (1987) relies on the use of dimensionless rate, q_D plotted against dimensionless time, t_D. Both q_D and t_D are divided by $[\ln\left(\frac{r_e}{r_{wa}}\right) - \frac{1}{2}]$ resulting in the "decline-curve dimensionless rate" q_{dD} and "decline-curve dimensionless time", t_{dD} in Equations 30 and 31 respectively (Fetkovich et al. 1987).

$$q_{dD} = \frac{141.2q(t)\mu B[\ln\left(\frac{r_e}{r_{wa}}\right)-\frac{1}{2}]}{kh(p_i - p_{wf})} \tag{30}$$

$$t_{dD} = \left[\frac{0.00634kt}{\Phi(\mu c_t)_i r_{wa}^2}\right]\left(\frac{1}{1/2[\left(\frac{r_e}{r_{wa}}\right)^2 -1][\ln\left(\frac{r_e}{r_{wa}}\right)-0.5]}\right) \tag{31}$$

In the equations above, t refers to the time, r_e/r_{wa} is the external boundary radius/effective wellbore radius, q is flow rate, p_i is the initial pressure, p_{wf} is the bottom hole flowing pressure, k is permeability and h is the reservoir thickness. In Figure 1.5, a schematic of the Fetkovich (1980) type curves demarcating transient flow and boundary dominated flow regimes for different r_e/r_{wa} values and b values.

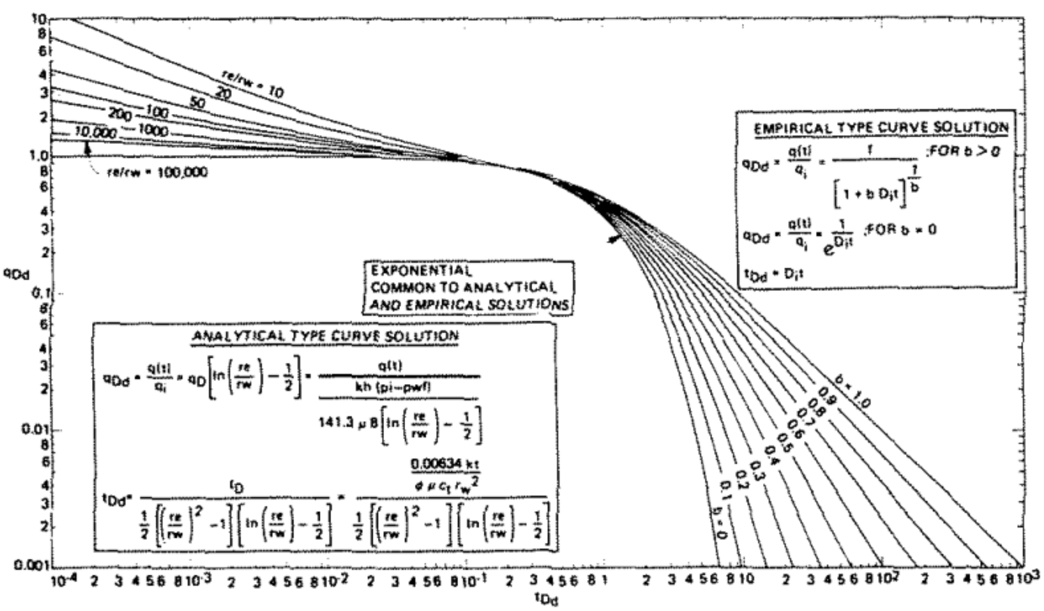

Figure 1.6— Composite of analytic and empirical type curves (Fetkovich 1980).

The Fetkovich (1980) type curves was created for a slightly compressible liquid assuming a constant $\mu_o c_o$ will be observed throughout the well's life.

"The accuracy in using the Fetkovich (1980) type curves for gas wells with large pressure drawdowns improved when dimensionless rate and cumulative production variables are defined in terms of real-gas pseudo pressure function" (Lee and Wattenbarger 1996, 222).

1.7 Improvements in Carter Type Curves over Other Methods of Production Data Analyses

The Fetkovich (1980) type curves is extended to the analysis of gas wells by defining the dimensionless rate and time variables in terms of the real-gas pseudo pressure function that incorporates the effect of changing gas properties (Fetkovich et al. 1987). Carter (1985) generated functions that include the changes in gas properties, $\mu_{g(p)}c_{g(p)}$ with pressure designed specifically for gas-well DCA. According to Lee and Wattenbarger (1996), Fetkovich (1980) type curves are used for modeling slightly compressible liquid and therefore assumes that the μc is constant over the life of the well.

Advantages of Carter (1985) over Fetkovich (1980) Type Curves

1. The correctness of Fetkovich (1980) type curves is based on its advancement for larger drawdown of gas wells because it can only be applied for limited boundary effects when the pressure transverse is small (Lee and Wattenbarger 1996, 223).

2.Carter (1981) work shows more precision than Fetkovich (1980) because the mathematical graphs and equations used the changes in gas properties with pressure (Lee and Wattenbarger 1996, 223).

3.They state that "Carter (1985) type curves was developed specifically for gas wells DCA and improves the accuracy by considering the variation of the $\mu_{g(p)}c_{g(p)}$ with average pressure" (Lee and Wattenbarger 1996, 220-223).

4. Carter (1985) is " the first to correlate rate/time behavior during boundary-dominated flow with a parameter, λ defined as the ratio of $\mu_{g(pi)}c_{g(pi)}$ to $\overline{\mu_g}\overline{c_g}$ evaluated at the average reservoir pressure, $\bar{p}$ and calculated as λ". The equation for λ is defined in Equation 6 above (Lee and Wattenbarger 1996, 222-223).

1.8 Limitation of Carter (1985) Type curves and Motivation for Work in this Thesis

Carter (1985) curves applied to constant-terminal-pressure-rate data from a single-phase liquid system such as an oil reservoir above the bubble point. However, there are no known mentions or applications of Carter (1985) type curves for multiphase flow. This can become especially challenging for complex fluids such as volatile oils, wet gases and gas condensate reservoirs. At pressures below the saturation pressure, multiphase flow occurs within the pore spaces of the rock. This influences the permeability to the oil or gas phases and additionally the compressibility and the viscosity of the fluids changes progressively over the life of the well. Consequently, it will become challenging to apply Carter (1985) type curves to production data analysis when these properties change rapidly.

In this thesis, I present an approach to estimate an effective fluid viscosity-compressibility product that will be valid for the entire life of the well for production both above and below the fluid saturation pressures. I then use these effective product values and correlate them with fluid C_{7+} values so that the practicing reservoir engineer can easily look-up values of the viscosity-compressibility product for use in the Carter (1985) type curves to forecast production and estimate EUR values.

1.9 Overview of Thesis

The major objective in this research is to calculate the Estimated Ultimate Recovery for shale wells for several different fluid types. The following describes the organization of the thesis.

Chapter One: The literature review discusses the progression of the first equations used for decline curve analysis, then Arps (1945) equations and Fetkovich (1980) type curves and their respective limitations and applications.

Chapter Two: The technical design of the reservoir grid used and the compositional modeling written in detail and all adaptations of reservoir engineering principles

Chapter Three: This is the methodology of the research describing the compositional modeling, the viscosity*compressibility for the multiplier co-efficient, graphical demonstration of the matching process and calculation of the t_D multipliers.

Chapter Four: The application of the type curves to fluid models. The procedure for compositional modeling, presentation of numerical solution using empirical approach for water model.

Chapter Five: The conclusions and recommendations observed from the results that could present more accurate values for the calculation of EUR.

Chapter Two: Reservoir Simulation Model Description

This chapter focuses on the reservoir model and fluid compositions used in this work to adapt Carter (1985) type curves for more complex fluids such as gas condensate and volatile oil reservoirs.

2.1 Reservoir Geometry

The reservoir simulation model used in this work is based on a 25x25x5 single porosity grid with widths of 30’, 30’ and 10’ in the x-, y- and z-directions respectively. The well in this model is a horizontal well intersected by four hydraulic fractures. The fractures are in a single plane with a fracture effective permeability of 50md, half-length of 250ft, width of 0.001ft. The fracture spacing is 120 ft. The wells are operated on a fixed bottom hole pressure constraint.

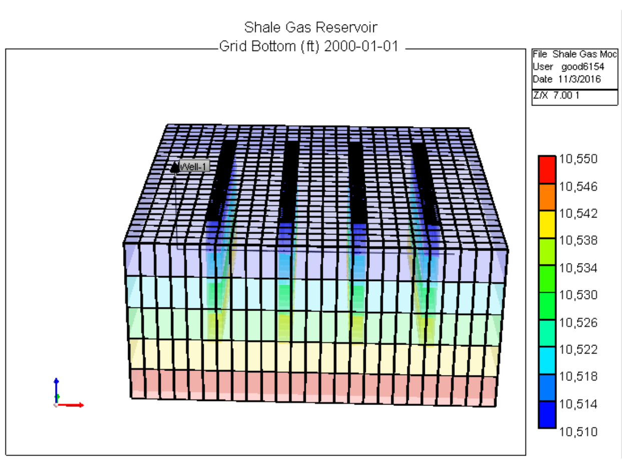

Figure 2.1—Reservoir grid block with planar fractures top of grid is 10500 to 10550ft.

Figure 2.1 shows a schematic of the reservoir model used in this study. The production rates output from the simulator used to compute EUR following the procedure outlined in Carter (1985).

2.2 Reservoir Well Constraints and Conditions

The reservoir grid has a reference pressure of 8000psi at the top of the reservoir at 10500ft. The bottom hole pressure (BHP) was limited to 6300psi for all the models for flow above the saturation pressure. For flow below the saturation pressure, the BHP was between 600 to 800 psi for gas wells and 2000 psi for volatile oil wells.

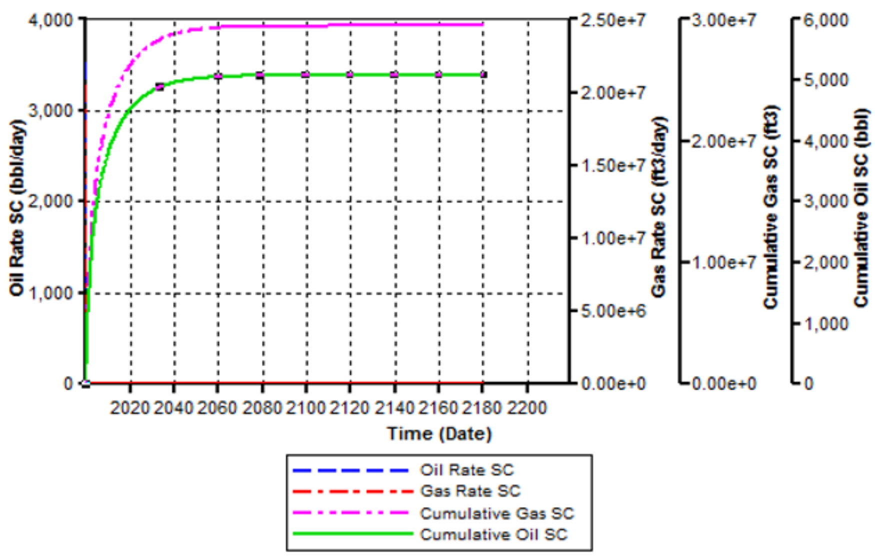

Figure 2.2— Simulator-derived production data and pressure of volatile well with cumulative oil production.The p_i is 8000psi and it declines to p_{wf} of 600psi.

2.3 Relative Permeability

Modeling wells, especially wet gases, requires the use of an appropriate relative permeability function and the most reliable model used for shale wells is the Corey's relative permeability model (Sanni and Gringarten 2008). The oil/gas relative permeability and the oil/water permeability plotted in Figure 2.3 and Figure 2.4.

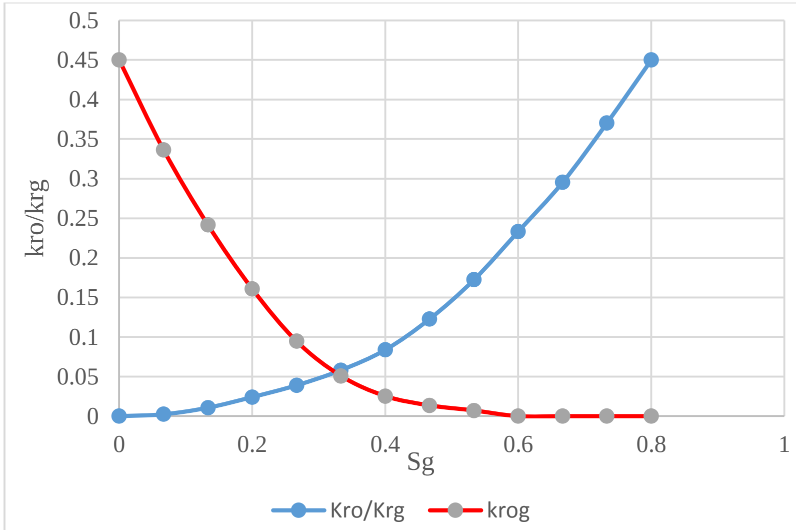

Figure 2.3–Relative permeability of gas and oil to gas adapted from a commercial simulator data file. Courtesy of Schlumberger.

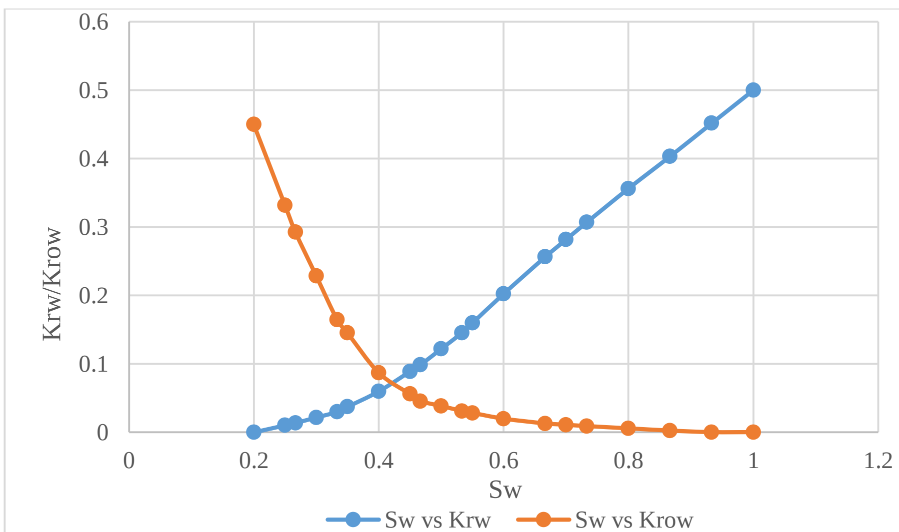

Figure 2.4–Relative permeability of water and water to oil, data from commercial simulator data file. Courtesy of Schlumberger.

2.4 PVT Data

The fluid compositions used in this study provided in Chapter 3. In this thesis, I have investigated several different fluid types ranging from dry gas to volatile oils with varying C_{7+} fractions.

Chapter Three: Methodology

This chapter utilizes the simulation results from the simulation model described in Chapter 2 for different types of fluids ranging from dry gases to black oils as a proxy for actual production data. The simulator output is plotted on the Carter (1985) type curves and I discuss the methodology adopted to estimate an effective viscosity-compressibility product for different fluid types.

3.1 Mathematical Multipliers

When computing the dimensionless rate and time, I use the fluid properties obtained from a compositional PVT package. The production data is then plotted on the Carter type curve. In order to obtain a match, the dimensionless time is adjusted by multiplying the $\mu_g c_g$ product with a multiplier, M. The equation for the dimensionless time t_D is:

$$t_D = \frac{2.634\text{x}10^{-4}\text{x}24kt}{\phi\mu(p_i)c_g(p_i)r_w^2}\alpha_1^2 \qquad (1)$$

3.2 Graphical Matching

The simulator production gas rate, q is multiplied by a quantity determined by trial and error resulting in production data that is adjacent to the type curves. The t_D ($\mu_g c_g$) multiplier is then applied next is to move the production data curve on the x-axis to overlap the type curves. The multiplier of q to q_D and t to t_D is used when calculating the EUR. In the entirety of the matching process, the priority of selecting the BDF regime over the transient flow period is paramount. In Figure 3.1, the Anderson volatile oil well adapted from Schenewerk and Heath (1989) has two different t_D with similar results, one has a better match in the boundary while the other matches better in the transient region.

3.3 Example of Graphical Match

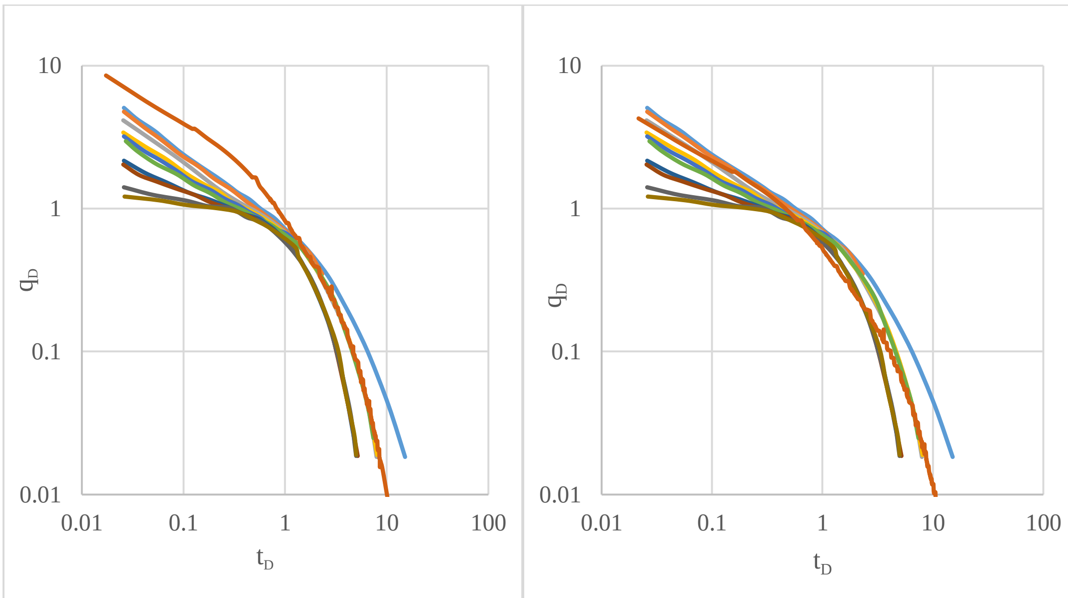

Fig 3.1—Production data from the Anderson volatile oil well (after Schenewerk and Heath 1989). The right graph has a better match for the transient region while the left has a better match for the boundary region.

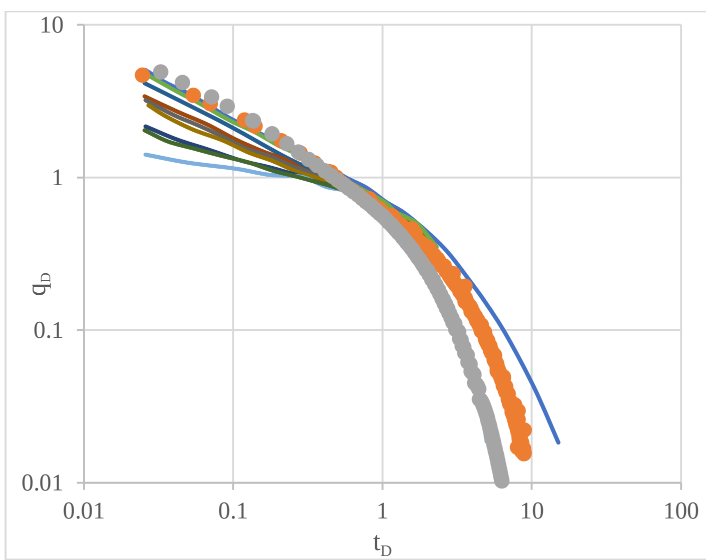

Figure 3.2— Simulator-derived production data for dry gas and wet gas matched on lambda = 0.55 and η=1.234 and lambda=0.75 and η=1.234 respectively.

3.4 Case Studies for Different Reservoir Fluids: Flow above Saturation Pressure

3.4.1 Water Case Study

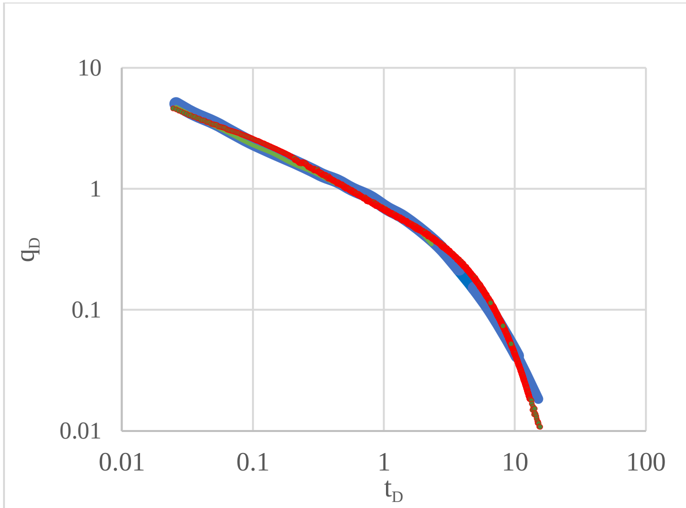

Figure 3.3— Simulator-derived production data for water matched on lambda=1.

The match of pure water on the λ=1 curve is shown in Figure 3.5.

Table 3.1— Fluid composition of water

Component	Water (mole fraction)
H_2O	100
C_{7+}	0

Table 3.2— Results obtained for water

Fluid Model	t_D multiplier (λ=1)	q_D multiplier (λ=1)	Rate Integral (λ=1)	EUR type curve calculated	Cumulative Production	% Error
Water	$1.5x10^{-4}$	2	3.5	1.7Mbbl	1.3 Mbbl	-7.7%

3.4.2 Wet Gas Case Study 1

The composition of wet gas 1 has a C_{7+} of 9.2% and the well operating conditions were p_i = 8000 psi and p_{wf} = 6300psi.The well is modeled as a single phase gas with no liquid production at reservoir and surface conditions. The fluid simulator laboratory tests gave a

$\mu_{g(pi)}c_{g(pi)}$ of 3.0×10^{-6} cp/psi (0.044 cp*6.7×10^{-5} 1/psi). This is used to calculate the t_D multiplier, of 2.8×10^{-4} for the λ=0.75 match and 2×10^{-4} for a λ=1 match. The q_D vs t_D integral is 2.7 and applied in calculations for the λ=0.75 match. A more accurate EUR is achieved with the λ=0.75 match which is best suited for a liquids-rich gas (Carter 1985).

Table 3.3— Results obtained for wet gas case study 1 EUR calculation.

Fluid Model	t_D multiplier (λ=0.75)	q_D multiplier (λ=1)	Rate Integral	EUR Calculated	Cumulative Production	% Error
Wet Gas 1	2×10^{-4}	1/3500	2.65	46.4 MMscf	42MMscf	+9.9%

Table 3.4— Fluid composition of wet gas1

Component	Wet Gas 1 (mole fraction)
CH_4	73.7
C_2H_6	9.5
C_3H_8	4.1
IC_4	2.0
NC_4	0.9
IC_5	0.6
NC_5	3.0
FC_6	0.6
C_7-C_9	0.6
C_{10}-C_{12}	5.0
Total C_{7+}	9.2

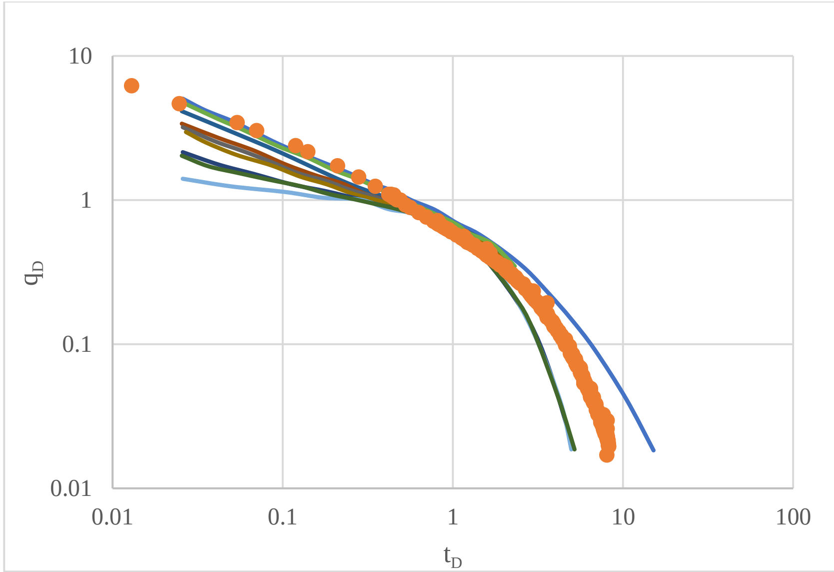

Figure 3.4— Simulator-derived production data for wet gas case study 1 matched on lambda = 0.75.

3.4.3 Dry Gas Case Study 1

The dry gas composition is 100% CH_4 is modeled with a p_{wf} = 6300psia.The data is well matched on a λ=0.55 type curve by adjusting $\mu_g c_g$ using a t_D multiplier to obtain a good match.

Table 3.5— Fluid Composition of dry gas 1

Component	Dry Gas (mole fraction)
CH_4	100
C_{7+}	0

Table 3.6— Results obtained for dry gas case study 1 EUR calculation.

Fluid	t_D multiplier (λ=0.55)	t_D multiplier (λ=1)	q_D multiplier	Rate Integral	EUR Calculated	Cumulative Production	% Error
Dry Gas 1	$1x10^{-4}$	_	1/3500	1.74	61 MMscf	72 MMscf	-18%
Dry Gas 1	_	$2.5x10^{-4}$	1/6500	2.69	70 MMscf	72 MMscf	-3%

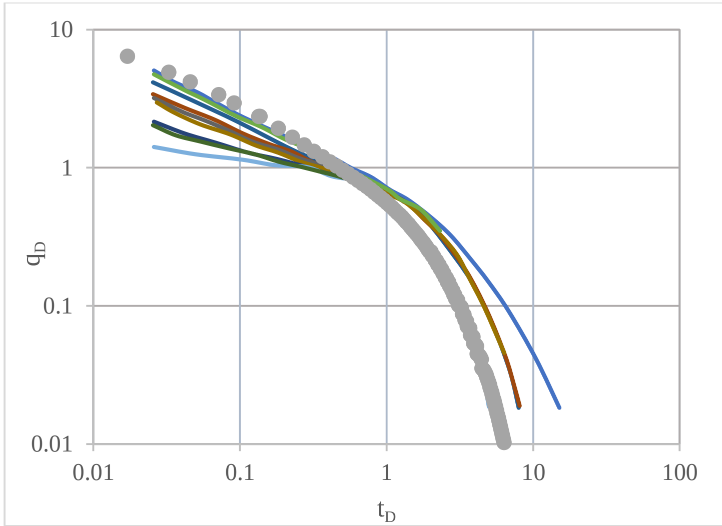

Figure 3.5— Simulator-derived production data of dry gas case study 1 matched on lambda=0.55.

3.4.4 Condensate Gas Case Study 1

The Condensate gas 1 has a C_{7+} fraction of 10% and was used in a reservoir with a p_i = 8000 psi and p_{wf} = 6300 psi. The fluid property data with the composition in shown in Table 3.7. The t_D multiplier is 2.8×10^{-4} for λ=1 match and 1.8×10^{-4} for λ=0.75 match. The rate integral, t_D and q_D multipliers are used to calculate the EUR and the λ=1 match gave the closest value to the simulator cumulative production data.

Table 3.7— Results obtained for condensate gas case study 1 for EUR calculation.

Fluid Model	t_D multiplier (λ=0.75)	t_D multiplier (λ=1)	q_D multiplier (λ=1)	Rate Integral	EUR Calculated	Cumulative Production	% Error
Condensate Gas 1	1.8×10^{-4}	2.8×10^{-4}	1/3500	2.14	27MMscf	30 MMscf	+10%

Table 3.8— Fluid composition of condensate gas 1 (courtesy CMG).

Component	Condensate 1 Mole Fraction
CO_2	0.01
N_2	0.1
CH_4	68.9
C_2H_6	8.6
C_3H_8	5.3
IC_4	1.2
NC_4	2.3
IC_5	0.9
NC_5	0.85
FC_6	1.73
C_7-C_9	4.69
C_{10}-C_{12}	2.12
C_{13}-C_{14}	1.37
C_{15}-C_{17}	0.82
C_{18+}	0.99
Total C_{7+}	10%

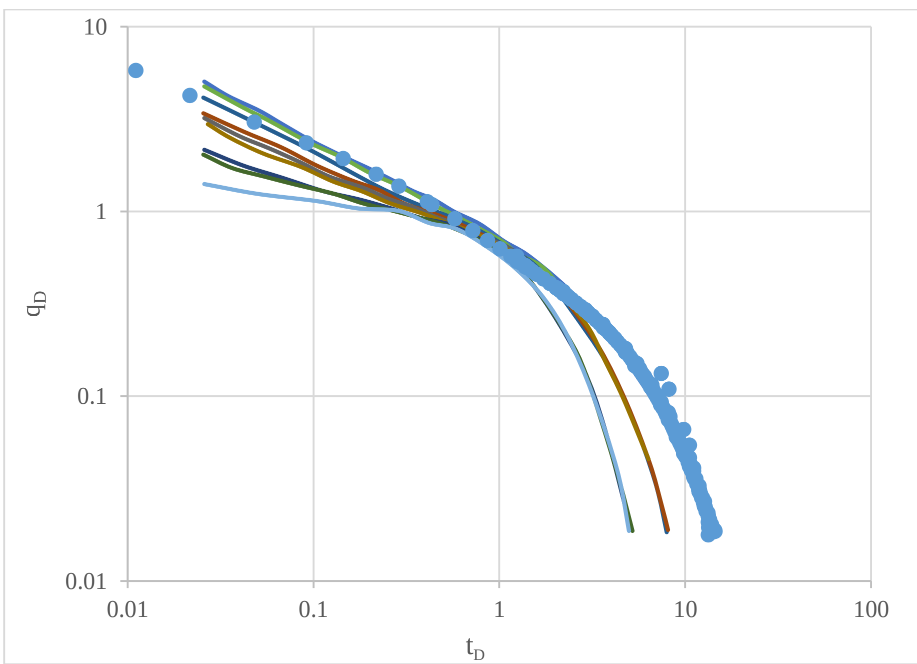

Figure 3.6— Simulator-derived production data for condensate case study 1 matched on lambda=1.

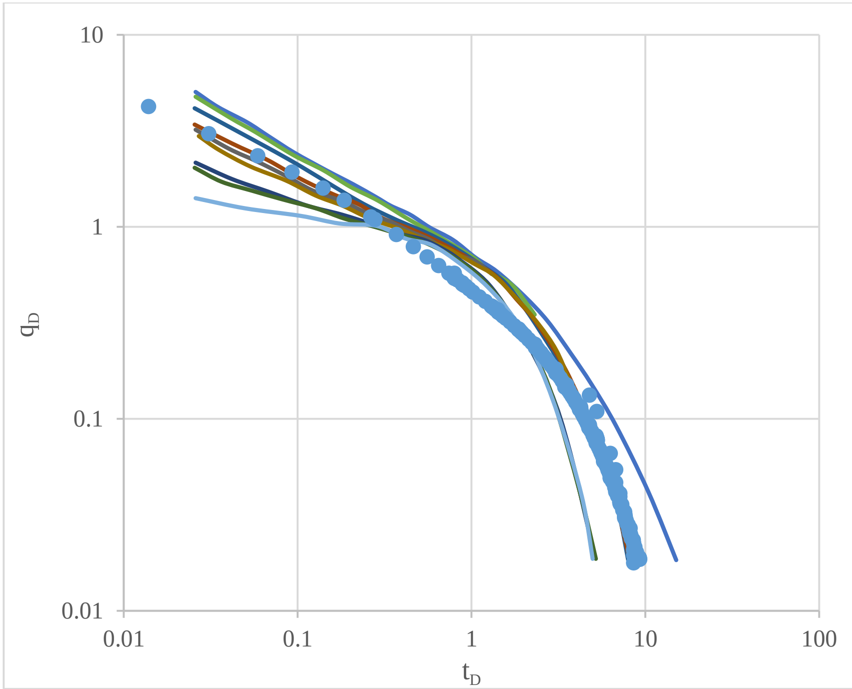

Figure 3.7— Simulator-derived production data for condensate case study 1 matched on lambda=0.75.

3.4.5 Volatile Oil Case Study 1

The composition of the volatile oil in Table 3.9 has an average C_{7+} fraction of 16.8%. The results of the match to λ=1 are given in the tables below.

Table 3.9— Fluid composition of volatile oil 1 (after Sanni and Gringaten 2008).

Component	Volatile oil 1 (mole fraction)
CO_2	0.9
N_2	0.1
CH_4	53.77
C_2H_6	11.46
C_3H_8	8.79
IC_4	4.56
IC_5	2.09
C_6	1.51
C_{7+}	16.92

Table 3.10— Results obtained for volatile oil case study 1 EUR calculation

Fluid Model	t_D multiplier (λ=1)	q_D multiplier (λ=1)	Rate Integral (λ=1)	EUR Calculated	Cumulative Production	% Error
Volatile oil 1	2.7×10^{-4}	1	2.48	4.96Mbbl	5.2 Mbbl	4.8%

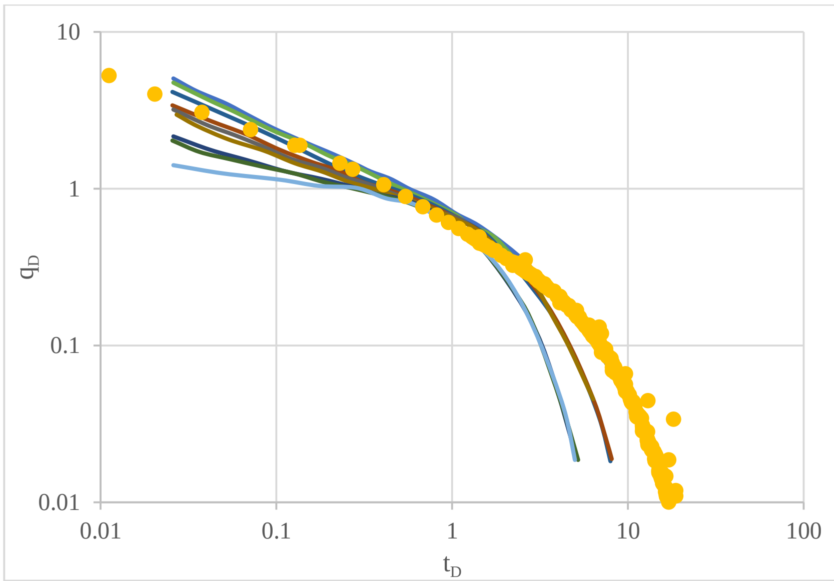

Figure 3.8— Simulator-derived production data of volatile oil case study 1 matched on lambda=0.75.

3.4.6 Volatile Oil Case Study 2

The fluid has a C_{7+} mole fraction of 23.9%. The results of the match to the curve with a λ=1 are provided in the tables below.

Table 3.11— Results obtained for volatile oil case study 2 for EUR calculations.

Fluid Model	t_D multiplier (λ=1)	q_D multiplier (λ=1)	Rate Integral (λ=1)	EUR Calculated	Cumulative Production	% Error
Volatile oil 2	1.2×10^{-4}	0.8	3.13	26Mbbl	24Mbbl	21%

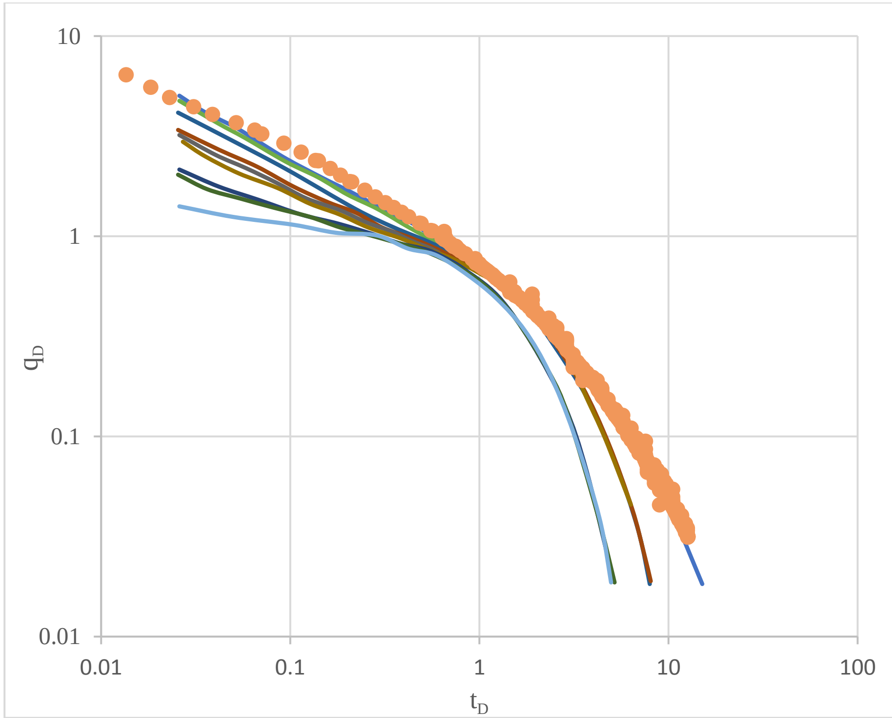

Figure 3.9─ Simulator-derived production data for volatile oil case study 2 matched on lambda=0.75.

3.4.7 Dry Gas Case Study 2

The dry gas has a C_{7+} fraction of 0% and is modeled at p_{wf}= 5000 psia. The data is well matched to λ=0.55 and 1. The $u_g c_g$ of 2.51×10^{-6} is used to calculate the t_D multiplier.

Table 3.12: Results obtained for dry gas case study 2 EUR calculations.

Fluid Model	t_D multiplier	q_D multiplier	Rate Integral	EUR Type Curve	Cumulative Production	% Error
Dry Gas 2 (λ=0.55)	2×10^{-4}	1/25000	2.14	267.5 MMscf	218.7 MMscf	18%
Dry Gas 2 (λ=1)	7×10^{-4}	1/50000	3.74	267.1 MMscf	218.7 MMscf	18%

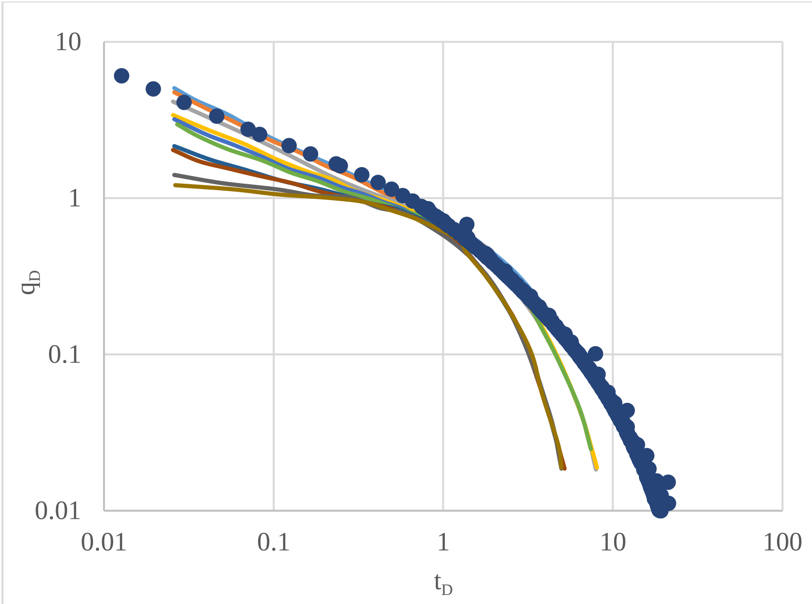

Figure 3.10— Simulator-derived production data for dry gas case study 2 matched on lambda =1.

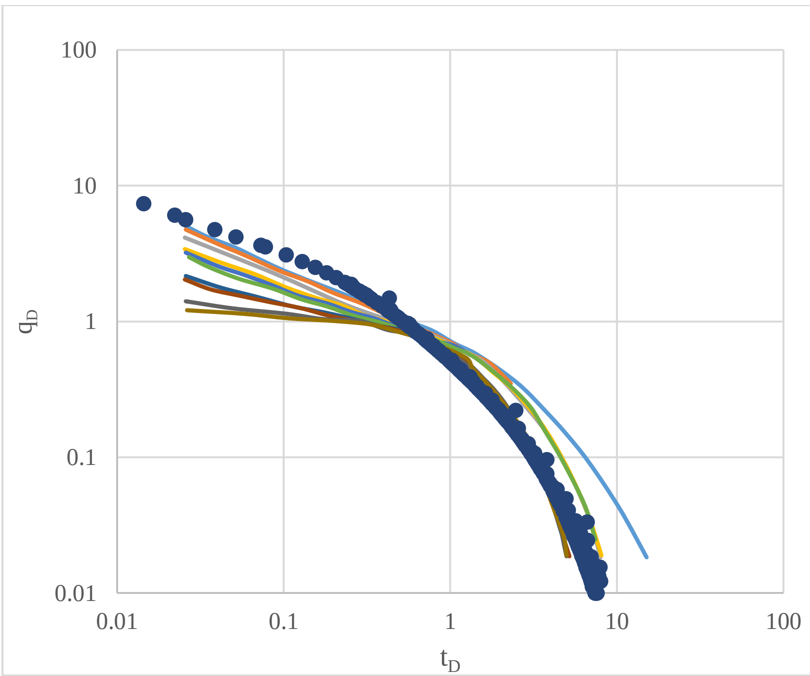

Figure 3.11— Simulator-derived production data for dry gas case study 2 matched on lambda=0.55.

3.4.8 Wet Gas Case Study 2

The wet gas 2 has a low C_{7+} fraction of 0.82%. The initial reservoir pressure, p_i=8000psi and the p_{wf} is 5000psi. The model production data matched to the type curves with a λ = 0.75, 1, and the results are shown in the tables below.

Table 3.13— Results obtained for wet gas case study 2 EUR calculations.

Fluid Model	t_D multiplier	q_D multiplier	Rate Integral	EUR Calculated	Cumulative Production	% Error
Wet Gas 2 (λ=0.75)	5x10^{-4}	1/40000	2.58	190 MMscf	197 MMscf	0.2%
Wet Gas 2 (λ=1)	9x10^{-4}	1/60000	2.22	148 MMscf	197 MMscf	28%

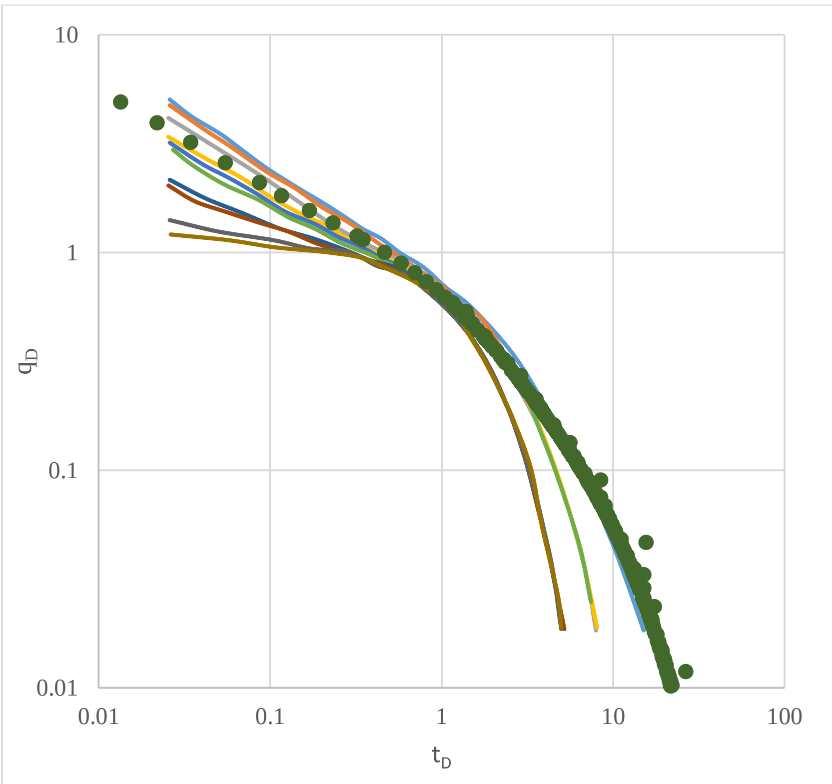

Figure 3.12— Simulator-derived production data for wet gas case study 2 matched on lambda=1.

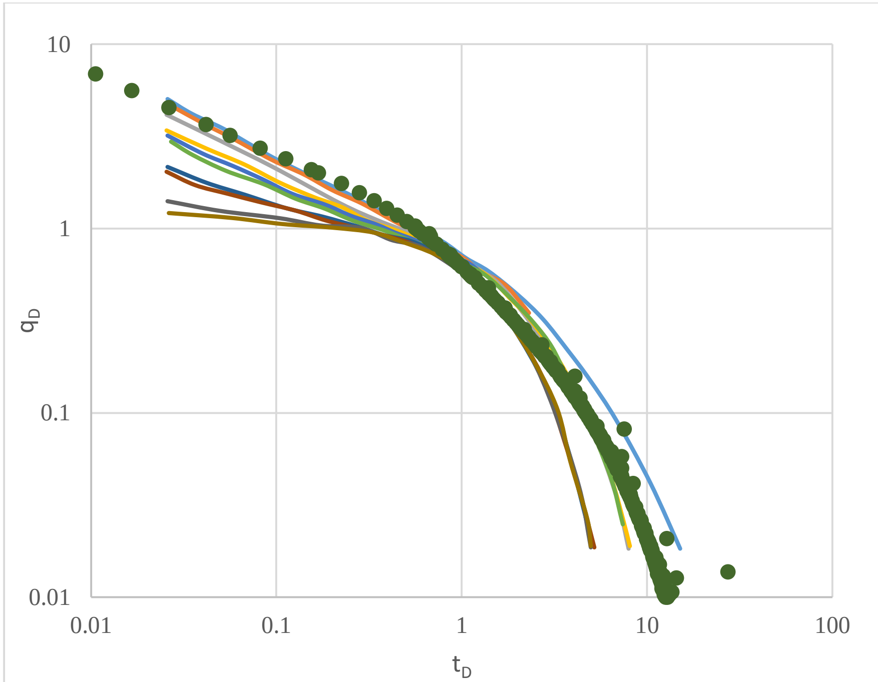

Figure 3.13— Simulator-derived production for wet gas case study 2 matched on lambda=1.

3.4.9 Condensate Gas Case Study 2

The condensate gas has a C_{7+} mole fraction of 12% which is taken from literature data and the model is run above saturation pressure using p_{wf} = 5000psi and p_i = 8000psi. The production data is matched to the type curve with a λ=1.

Table 3.14— Results obtained for condensate gas case study 2 EUR calculations.

Fluid Model	t_D multiplier	q_D multiplier	Rate Integral	EUR Calculated	Cumulative Production	% Error
Condensate 2 λ=0.75	4.5x10^{-4}	1/16000	2.37	84.3 MMscf	70MMscf	+17%
Condensate 2 λ=1	7 x10-4	1/16000	3.05	69.7 MMscf	70MMscf	0.4%

Table 3.15— Fluid Composition of condensate gas 2

Component	Condensate 2 (mole fraction)
CO_2	0.9
N_2	0.7
CH_4	62.4
C_2H_6	11.8
C_3H_8	5.5
IC_4	1.3
NC_4	2.1
IC_5	1.2
NC_5	1.0
C_6	1.2
C_7	1.8
C_8	2.3
C_9	1.7
C_{10}	6.1

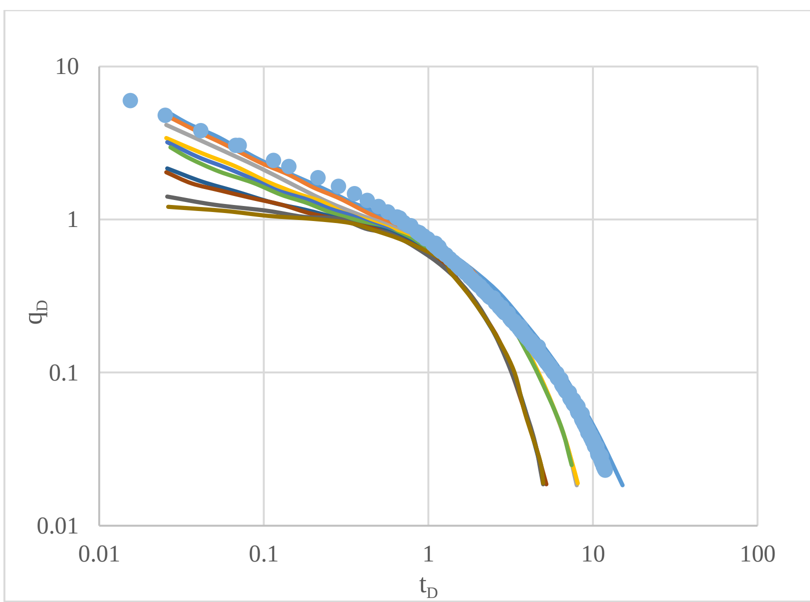

Figure 3.14—Simulator-derived production condensate gas case study 2 matched on lambda=1.

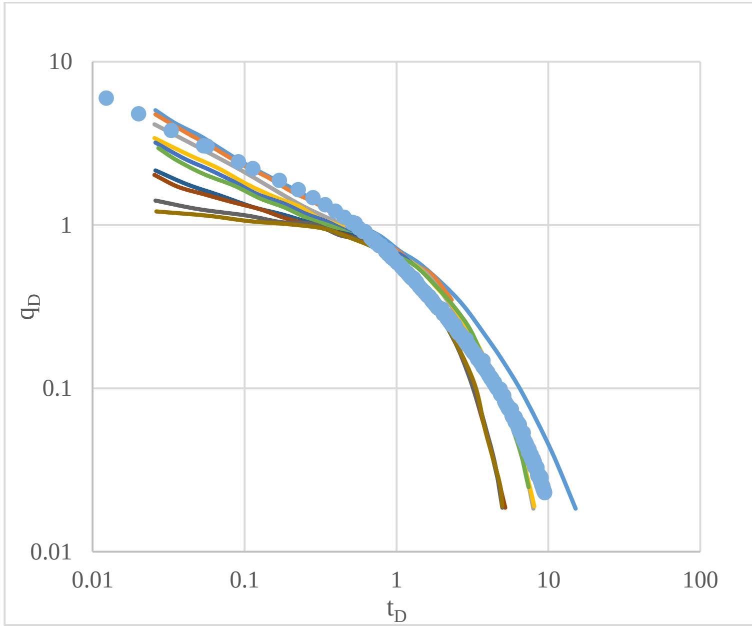

Figure 3.15— Simulator-derived production condensate gas case study 2 matched on lambda=0.75.

3.4.10 Volatile Oil Case Study 3

The C_{7+} mole of fraction of the volatile oil is 21.76% and the well is modeled with a p_i=8000psi and a p_{wf}=5000psi. The results of the match shown in the figures and tables below.

Table 3.16— Results obtained for volatile oil case study 3 EUR calculation.

Fluid Model	t_D multiplier	q_D multiplier	Rate Integral	EUR Calculated	Cumulative Production	% Error
Volatile oil 3 (λ=1)	$8x10^{-4}$	2.5	3.8	11.9 Mbbl	11.7Mbbl	+2%

Table 3.17— Fluid composition for volatile oil 3 (courtesy CMG)

Component	Volatile oil 3 (mole fraction)
CO_2	0.9
N_2	0.2
CH_4	58.8
C_2H_6	7.6
C_3H_8	4.1
IC_4	0.9
NC_4	2.1
IC_5	0.8
NC_5	1.2
C_6	1.8
C_{7+}	21.8

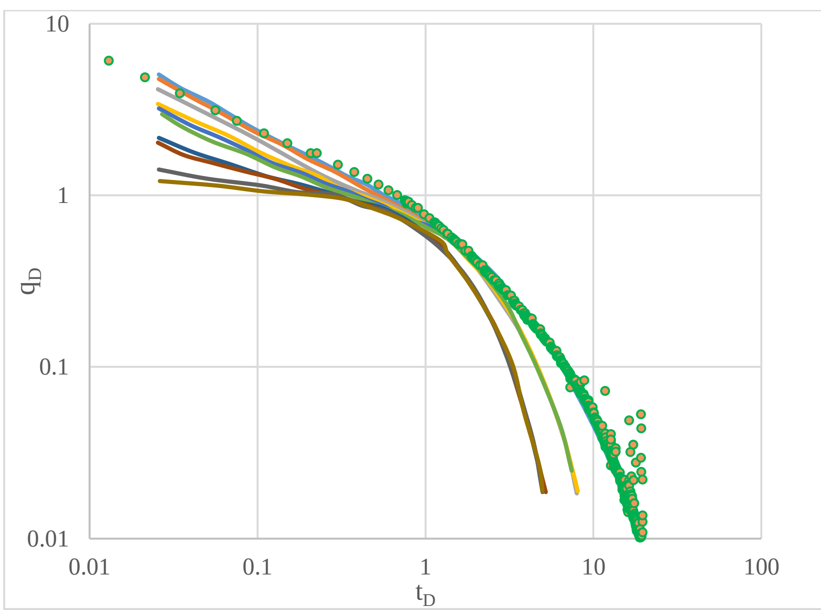

Figure 3.16— Simulator-derived production data for volatile oil case study 3 matched on lambda= 1.

3.4.11 Wet Gas Case Study 3

The Spivey and McCain (2013) field data for wet gas was modeled at a p_i= 8000psi and a p_{wf}=5000psi. The results of the match shown in the tables below.

Table 3.18— Results obtained for wet gas case study 3 EUR calculation

Fluid Model	t_D multiplier	q_D multiplier
Wet Gas 3 λ=0.75	$8x10^{-4}$	1/10000
Wet Gas 3 (λ=0.55)	2.5x10-4	1/5000

Table 3.19— Fluid composition for wet gas 3 (after Spivey and McCain,2013)

Component	Wet Gas 3 (mole fraction)
H_2S	0.46
CO_2	1.82
N_2	0.91
CH_4	81.11
C_2H_6	3.65
C_3H_8	3.01
IC_4	2.79
IC_5	1.57
C_6	1.28
C_{7+}	3.41

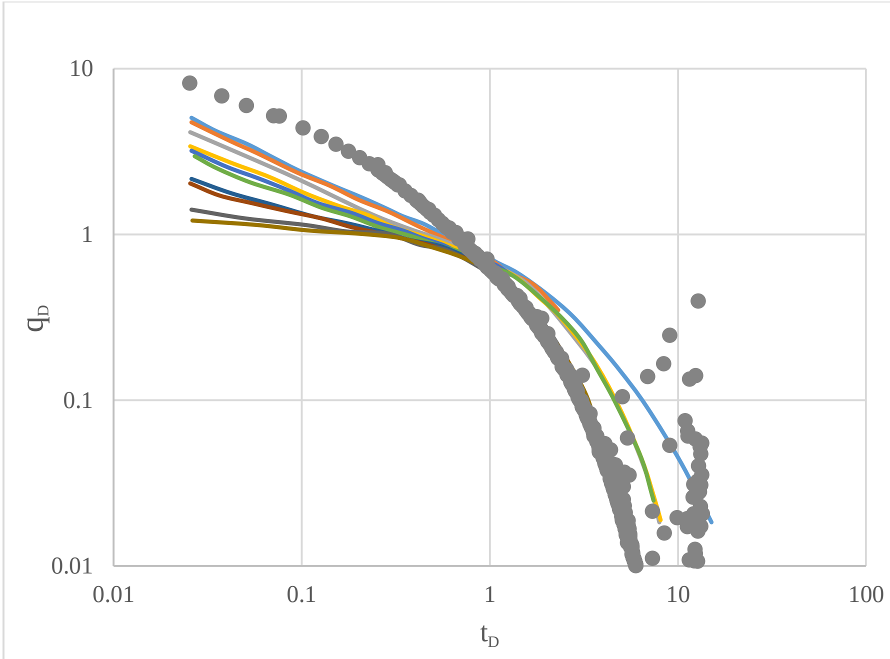

Figure 3.17— Simulator-derived production data for wet gas case study 3 matched on lambda=0.55.

3.5 Case Studies for Flow below the Fluid Saturation Pressure

3.5.1 Condensate Gas Case Study 1

The condensate fluid has a C_{7+} composition of 10% with a p_i=8000psi and p_{wf}=600psi. The matches to the type curves shown in the Figure 3.18, Figure 3.19 and Table 3.20 below.

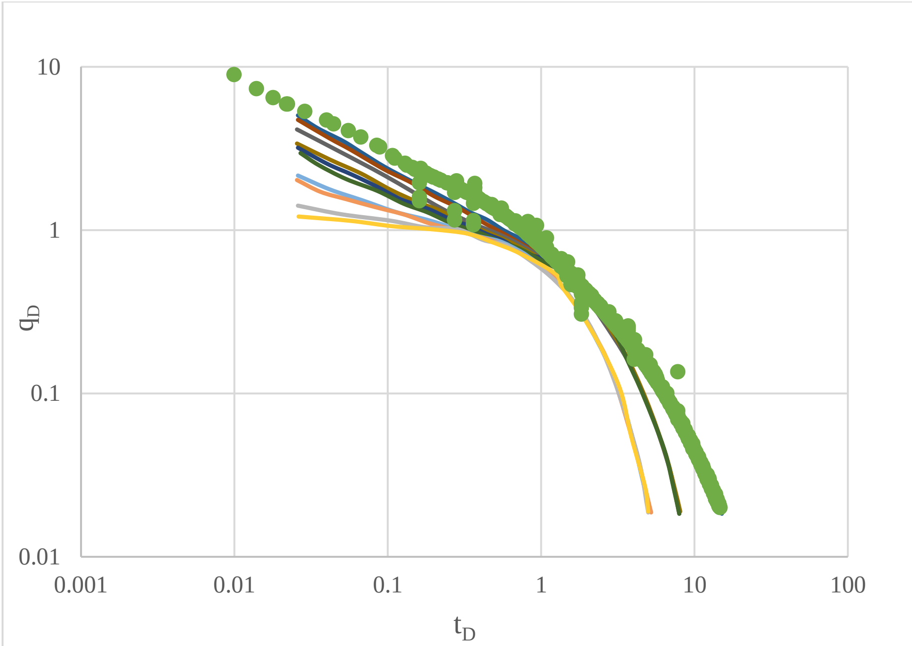

Figure 3.18— Simulator-derived production data for volatile oil case study 2 matched on lambda=1.

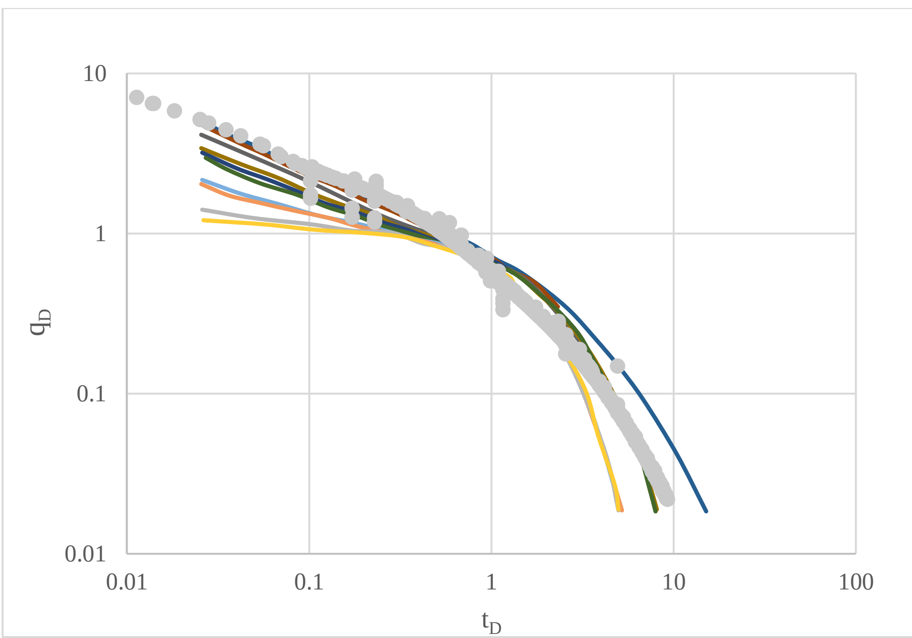

Figure 3.19—Simulator-derived production data for condensate case study 1 matched on lambda=0.75.

Table 3.20— Results obtained for condensate case study 1 EUR calculation.

Fluid Model	t_D multiplier (λ=1)	t_D multiplier (λ=0.75)	q_D multiplier (λ=1)	Rate Integral (λ=1)	EUR type curve	Cumulative Production	% Error
Condensate Gas 1	2.2x10^{-4}	1.5x10^{-4}	5x10^{-5}	2.14	29.6Mbbl	28.6Mbbl	3.71%

3.5.2 Wet Gas Case Study 1

The composition has a total C_{7+} of 9.2% and the operating conditions are p_i=8000psi and p_{wf}=600psi. The matches to the type curves are shown in the figures and tables below.

Table 3.21— Results obtained for wet gas case study 1 EUR calculation.

Fluid Model	t_D multiplier (λ=1)	t_D multiplier (λ=0.75)	q_D multiplier (λ=1)	Rate Integral	EUR Calculated	Cumulative Production	% Error
Wet gas 1	6.2x10^{-4}	3.5x10^{-4}	1x10^{-6}	2.65	44 MMscf	42.7MMscf	3.0 %

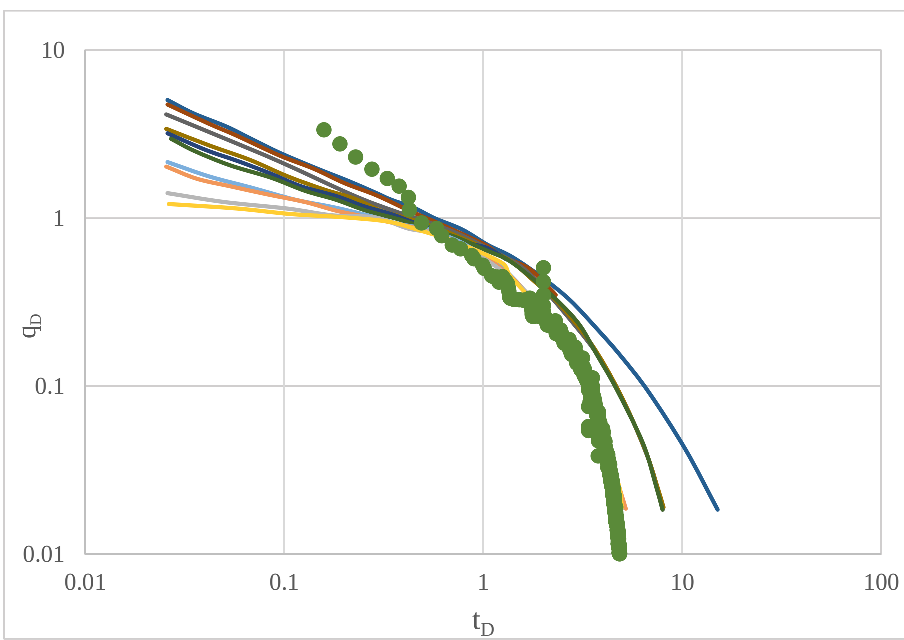

Figure 3.20— Simulator-derived production data for wet gas case study 1 matched on lambda=0.55.

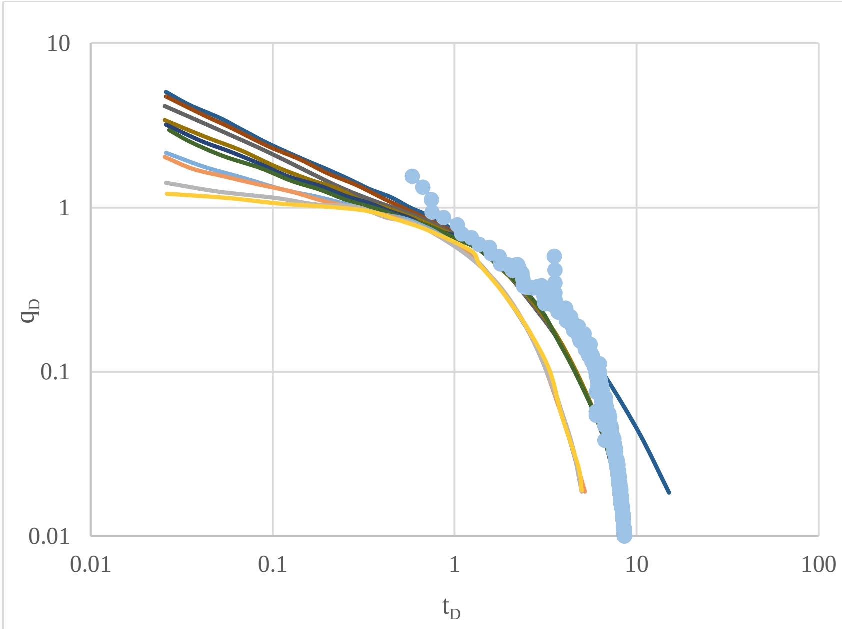

Figure 3.21— Simulator-derived production data for wet gas case study 1 matched on lambda =0.75.

3.5.3 Volatile Oil Case Study 3

The C_{7+} mole fraction is 23.9% and the matches to the type curve with a λ=1 are shown in the figures and tables below.

Table 3.22— Results obtained for volatile oil case study 3 EUR calculation.

Fluid Model	t_D multiplier (λ=1)	q_D multiplier (λ=1)	Rate Integral (λ=1)	EUR Calculated	Cumulative Production	% Error
Volatile oil 2	5 x10^{-4}	3	3.8	23Mbbl	2.8Mbbl	24 %

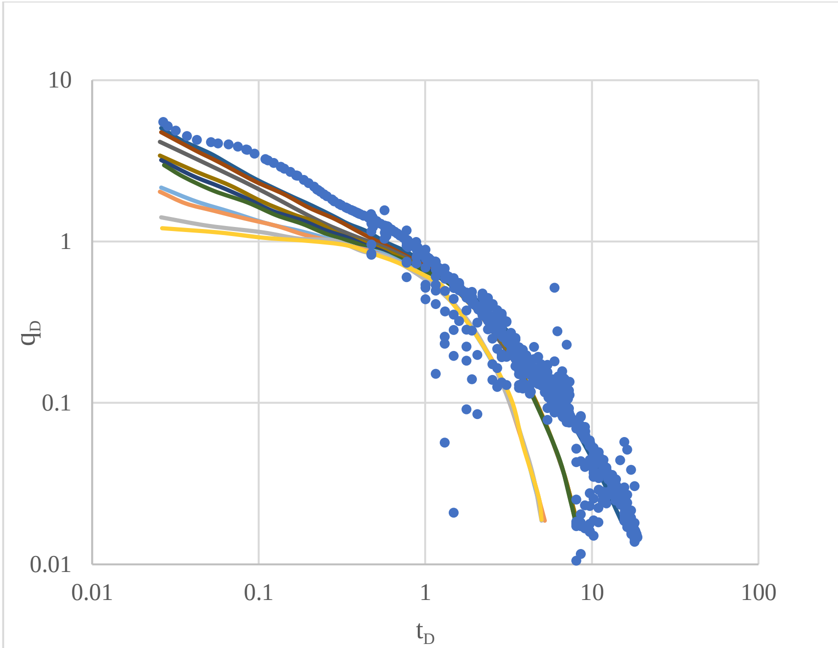

Figure 3.22— Simulation-derived production data for volatile oil case study 3 matched on lambda=0.75.

3.5.4 Dry Gas Case Study 1

The dry gas model discussed here operated with a p_{wf} of 800psi. The match to the type curve with a λ=1 gave a more accurate EUR of 384.3 MMscf and the results are shown in the figures and tables below.

Table 3.23— Results obtained for dry gas case study 1 EUR calculation.

Fluid Model	t_D multiplier (λ=1)	t_D multiplier (λ=0.55)	q_D multiplier (λ=1)	Rate Integral (λ=1)	EUR Calculated	Cumulative Production	% Error
Dry Gas 1	$3.5\text{x}10^{-4}$	$2\ \text{x}10^{-4}$	1/50000	2.69	384.3MMscf	402.3 MMscf	4.68 %

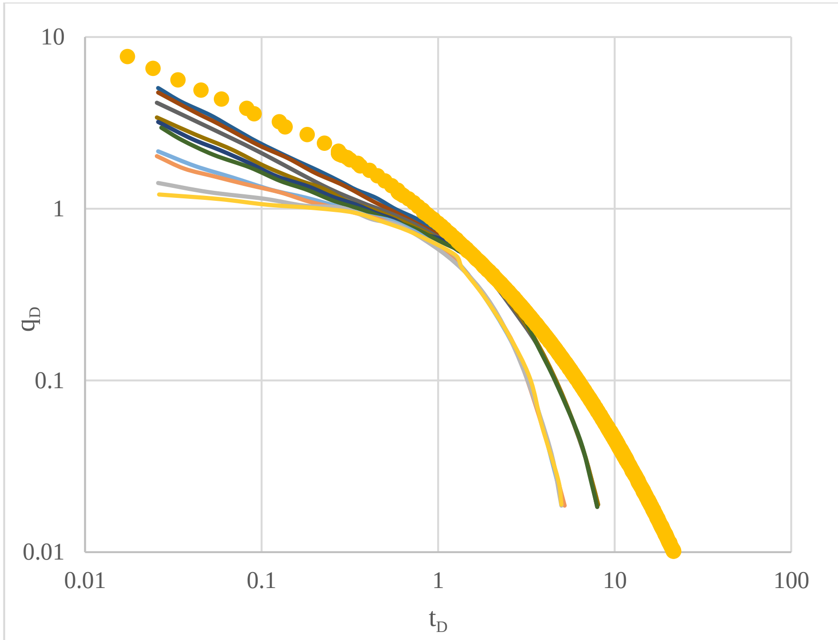

Figure 3.23— Simulation-derived production data for dry gas case study 1 matched on lambda=0.75.

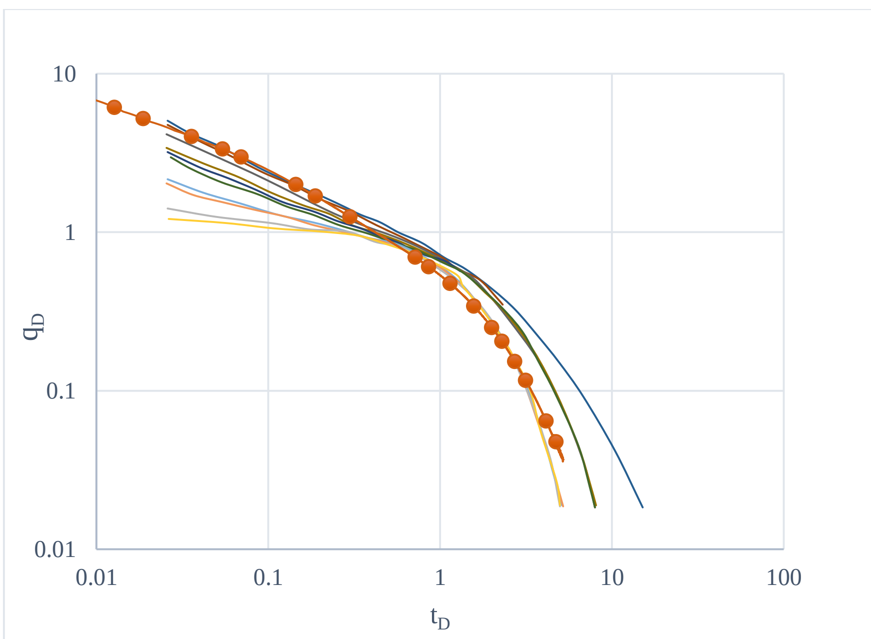

Figure 3.24— Simulator-derived production data for dry gas case study 1 matched on lambda=0.55.

3.5.5 Condensate Gas Case Study 2

The condensate gas well operates at a p_{wf} of 800psi with a pi of 8000psi. The matches to the type curves is shown in the figures and tables below.

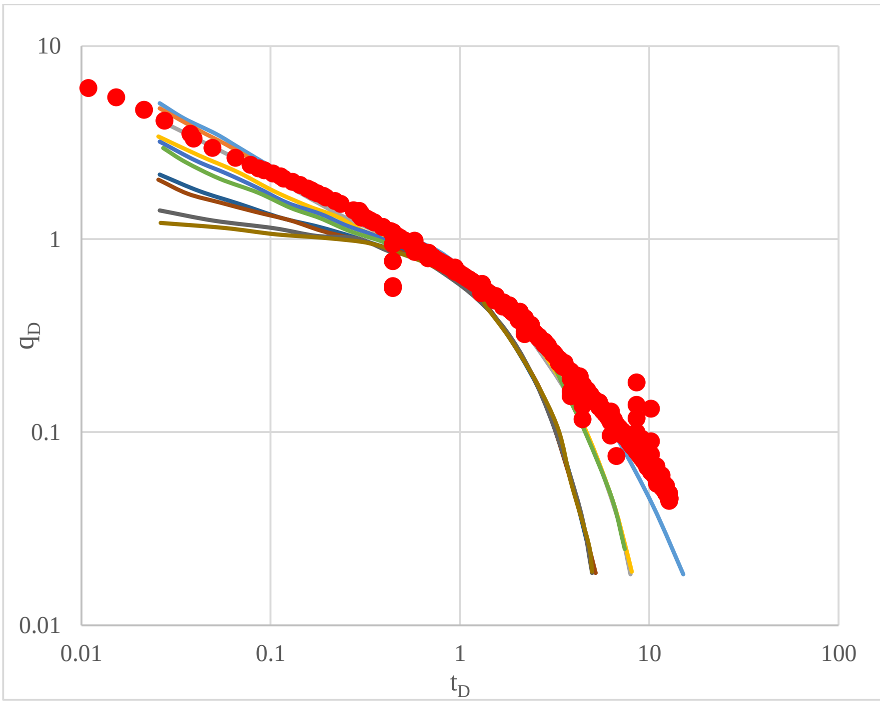

Figure 3.25— Simulator- derived production data for condensate case study 2 matched on lambda=1.

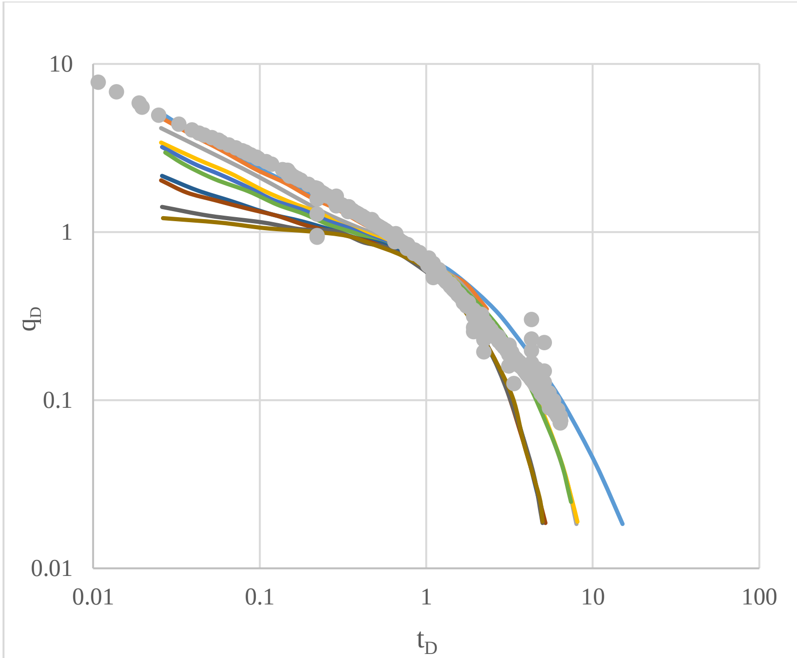

Figure 3.26— Simulation-derived production data for condensate gas case study 2 matched on lambda=0.75.

Table 3.24— Results obtained for condensate gas case study 2

Fluid Model	t_D multiplier	q_D multiplier	Rate Integral	EUR Calculated	Cumulative Production	% Error
Condensate Gas2 (λ=0.75)	2.2x10^{-4}	1/22000	2.65	265 MMscf	248MMscf	+6.4%
Condensate Gas 2 (λ=1)	3.6x10^{-4}	1/30000	3.19	266 MMscf	248MMscf	+6.8%

3.5.6 Volatile Oil Case Study 2

The C_{7+} mole fraction is 23.9% with the operating conditions of $p_{i=}$8000psi and p_{wf} of 600psi for modeling below the fluid saturation pressure. The matches to the type curves are shown in the figures and tables below.

Table 3.25— Results obtained for volatile oil case study 2 EUR calculation.

Fluid Model	t_D multiplier	q_D multiplier	Rate Integral	EUR Calculated	Cumulative Production	% Error
Volatile Oil 2	1.2×10^{-4}	1.5	3.59	44.8Mbbl	46.5Mbbl	3.80%

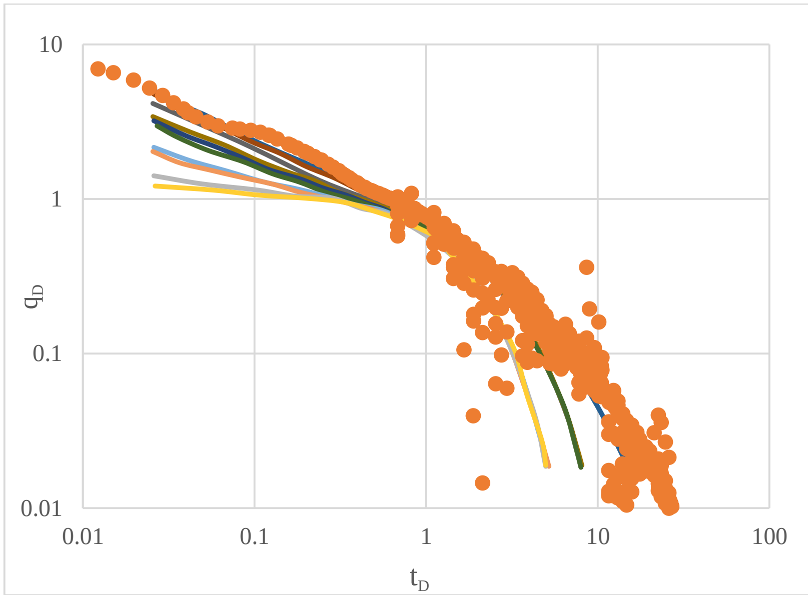

Figure 3.27— Simulator-derived production data for volatile oil case study 2 matched on lambda=1.

3.5.7 Wet Gas Case Study 2

The composition has a total C_{7+} of 0.82% and the well was operated with a p_i= 8000psi and p_{wf} = 800psi. The matches to the type curves are shown in the figures and tables below for λ=0.75 and λ=1.

Table 3.26— Results obtained for wet gas case study 2 EUR calculation.

Fluid Model	t_D multiplier	q_D multiplier	Rate Integral	EUR Calculated	Cumulative Production	% Error
Wet gas 2 (λ=0.55)	1.2×10^{-4}	1/32000	1.88	503 MMscf	432MMscf	16%
Wet gas 2 (λ=1)	4x10-4	1/60000	3.40	510 MMscf	432MMscf	18%

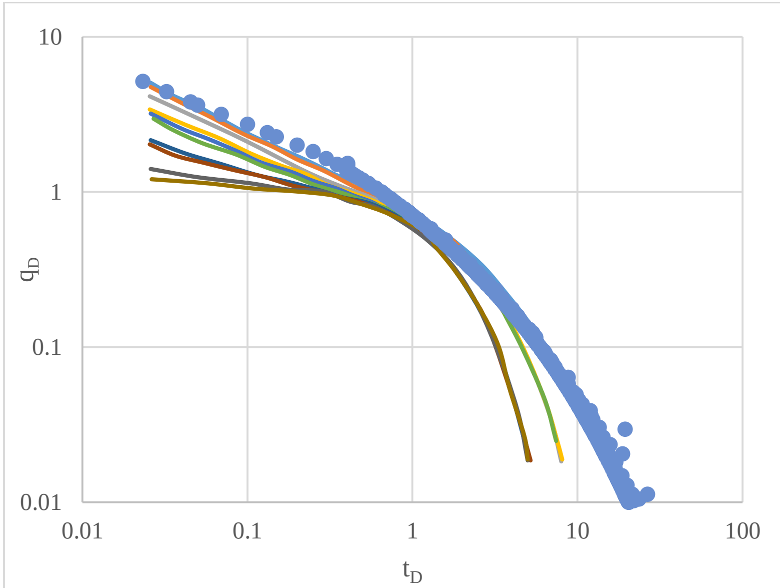

Figure 3.28— Simulation – derived production data for wet gas case study 2 matched on λ=1.

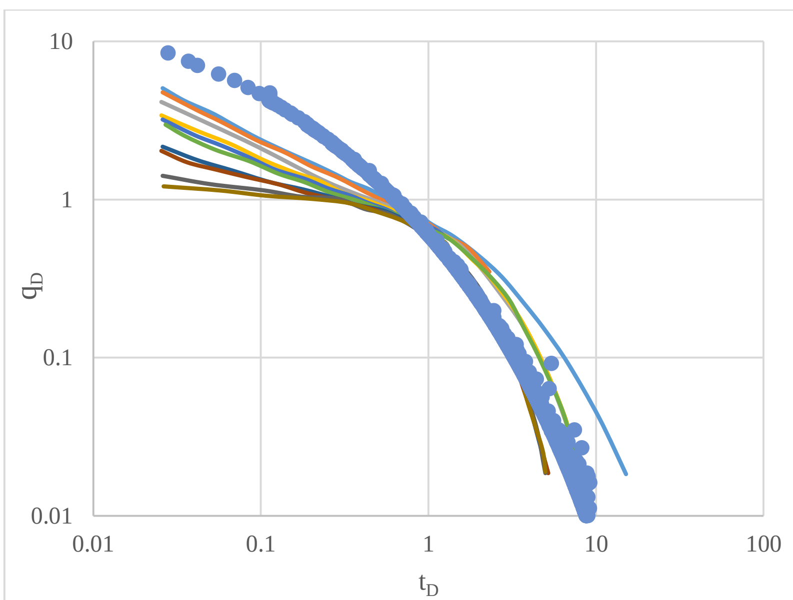

Figure 3.29— Simulation – derived production data for wet gas case study 2 matched on λ=0.55.

3.5.8 Dry Gas Case Study 2

The dry gas has a C_{7+} fraction of 0% and is modeled at p_{wf} = 800 psia. The matches to the type curves are shown in the figures and tables below for λ=0.55 and λ=1.

Table 3.27— Results obtained for dry gas case study 2 EUR calculation.

Fluid Model	t_D multiplier	q_D multiplier	Rate Integral	EUR Calculated	Cumulative Production	% Error
Dry gas 2 (λ=0.55)	2.05×10^{-5}	1/20000	2.66	259 MMscf	219MMscf	15%
Dry gas 2 (λ=1)	5.8×10^{-4}	1/45000	3.44	267 MMscf	219 MMscf	17%

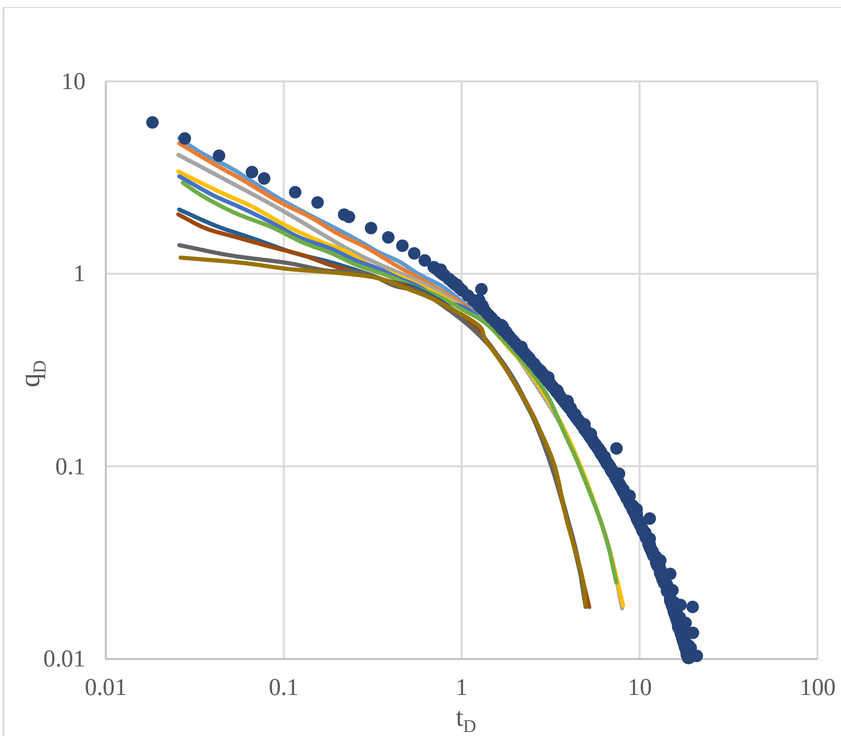

Figure 3.30— Simulator-derived production for dry gas case study 2 matched on lambda = 1.

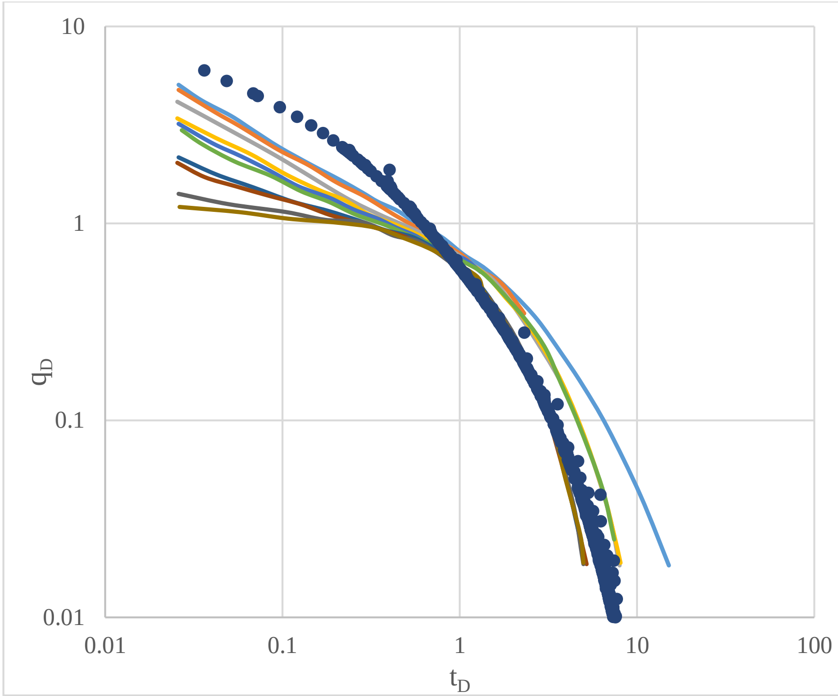

Figure 3.31— Simulator-derived production for dry gas case study 2 matched on lambda = 0.55.

3.5.9 Volatile Oil 3 Case Study

The C_{7+} mole fraction of the volatile oil is 21.8%. The well is modeled with a p_i=8000psi and p_{wf}=800psi. The matches to the type curves are shown in the figures and tables below for λ=1.

Table 3.28—Results obtained for volatile oil case study 3 EUR calculation.

Fluid Model	t_D multiplier	q_D multiplier	Rate Integral	EUR type curve	Cumulative Production	% Error
Volatile Oil 3	5x10^{-4}	1	3.13	26.1Mbbl	24.1Mbbl	21%

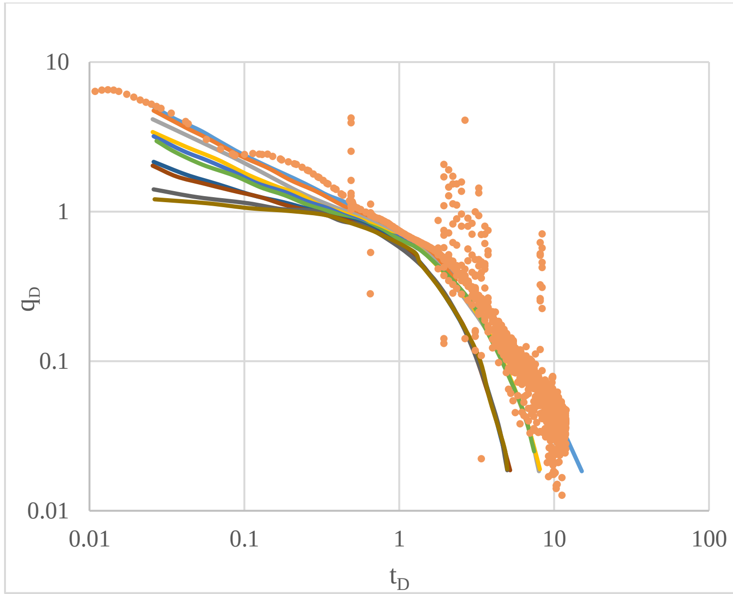

Fig 3.32— Simulator- derived production data for volatile oil case study 3 matched to lambda= 1.

3.5.10 Wet Gas Case Study 2

The wet gas 2 has a low C_{7+} composition of 0.82%. The well operated with a p_i of 8000psi and p_{wf} of 800psi. The matches to the type curves are shown in the figures and tables below for λ=0.55 and λ=1.

Table 3.29— Results obtained for wet gas case study 2 EUR calculation.

Fluid Model	t_D multiplier	q_D multiplier	Rate Integral	EUR Calculated	Cumulative Production	% Error
Wet gas 2 (λ=0.55)	1.2x10^{-4}	1/32000	1.88	503MMscf	422 MMscf	+16%
Wet gas 2 (λ=1)	4 x10^{-4}	1/60000	3.40	510MMscf	422 MMscf	+17%

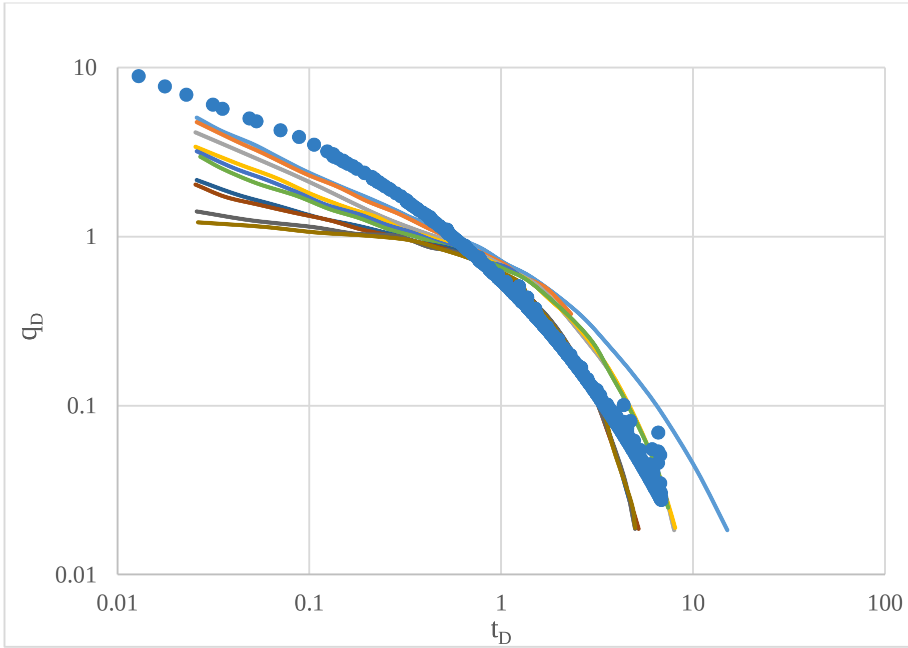

Fig 3.33— Simulator-derived production data for wet gas case study 2 matched on lambda=0.55.

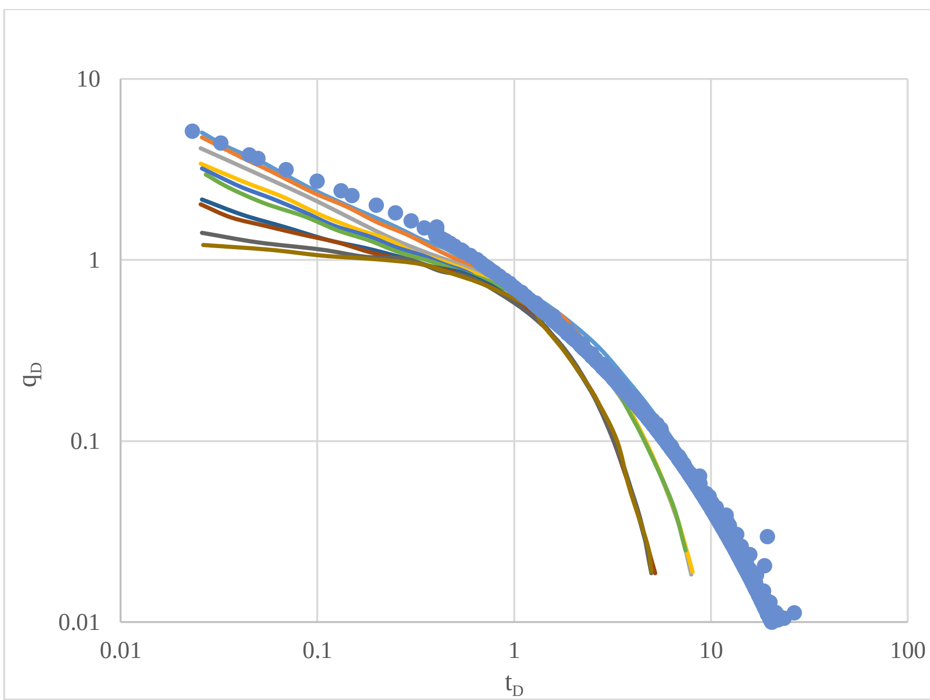

Fig 3.34— Simulator- derived production data for wet gas case study 2 matched on lambda=1.

3.6 Estimated Ultimate Recovery

The calculation of the Estimated Ultimate Recovery (EUR) requires the rate integral which corresponds to the area under the curve in the Carter type curves.

3.7 Analytical Calculations of EUR

The Carter (1985) approach to estimating recoverable gas content, G_p tested with different fluid models. The recoverable gas present in the reservoir for a drawdown of p_i-p_{wf} using Equation 8:

$$\Delta G = G_{(p_i)} - G_{(p_{wf})} = \frac{qt\eta}{\lambda q_D t_D} \tag{8}$$

$$\Delta G = G_{(p_i)} - G_{(p_{wf})} = \frac{\left(\frac{p}{z}\right)_i}{\left(\frac{p}{z}\right)_i - \frac{P}{z_{(p_{wf})}}} \tag{9}$$

The results for three different fluid models shown in Table 3.45 below.

Table 3.30— $G_{(pi)}$ of models below Saturation Pressure

Fluid Model	$\mu_g c_g$ at 8000psi	$\mu_g c_g$ at 800psi	$G_{(pi)}$
Dry Gas 2 (λ=0.55)	2.51E-06	2.76E-05	164 MMscf
Wet Gas 2 (λ=0.55)	2.55E-06	1.86E-05	41.4 MMscf
Condensate 2 (λ=0.75)	2.72E-06	6.85E-07	181 MMscf

In the next chapter, I have combined all the results obtained in this chapter to generate a correlation between the viscosity-compressibility product and the fluid C_{7+} fractions.

Chapter Four: Compilation of Results

In this chapter, I compiled the results presented in Chapter 3 for each of the different case studies. In Chapter 2, I discussed the procedure to obtain an equivalent viscosity-compressibility product using reservoir simulation for a diverse range of fluids for production both above and below the fluid saturation pressures. I also presented the EUR calculations using the Carter (1985) type curves for each of these fluid types.

4.1 Case Studies for Production above the Saturation Pressure

Table 4.1 presents the compiled results for the t_D multiplier (viscosity-compressibility multiplier) as well as the q_D multiplier against the C_{7+} fractions.

Table 4.1−Calculated multiplier for fluid models above saturation pressure.

Fluid Composition	t_D Multiplier ($x10^{-4}$)	q_D Multiplier	C_{7+} mole fraction
Volatile Oil 2	1.2	0.8	24
Volatile Oil 1	5.0	1	16.8
Condensate1 (λ=0.75)	1.8	1/3500	11.7
Condensate 1	2.8	1/3500	11.7
Wet Gas1 (λ=0.75)	2	1/3500	9.2
Wet Gas1	2.8	1/3500	9.2
Dry Gas1 (λ=0.55)	1.2	1/6500	0
Dry Gas1	2.5	1/6500	0
Water	1.5	2	0
Dry Gas 2 (λ=1)	7.0	1/50000	0
Dry Gas 2 (λ=0.55)	2.0	1/25000	0
Wet Gas 2 (λ=1)	9.0	1/60000	0.82
Wet Gas 2 (λ=0.75)	5.0	1/40000	0.82
Condensate 2 (λ=1)	7.0	1/16000	6.1
Condensate2(λ=0.75)	4.5	1/16000	6.1
Volatile Oil 3	8.0	2.5	21.8
Armstrong λ=1 **(**Schenewerk and Heath 1989)	8	1	19.4
Armstrong λ=0.75**(**Schenewerk and Heath 1989)	6	1	19.4
Anderson λ=1**(**Schenewerk and Heath 1989)	8	1	18.4
Anderson λ=0.75 **(**Schenewerk and Heath 1989)	5	2	18.4
Wet Gas 3 λ=0.55(Spivey and McCain,2013)	2.5	1/5000	3.4
Wet Gas3 λ=0.75 (Spivey and McCain,2013)	8	1/10000	3.4

Table 4.2 provides a list of values of predicted EUR for the wells with the given fluid compositions. The term AUC refers to Area under the Curve.

Table 4.2—Mathematical simulator calculations of the rate integral termed area under the matched curve (AUC) for q vs t above saturation pressure.

Fluid Composition	EUR AUC q vs t
Volatile Oil 2	$2.2x10^4$
Volatile Oil 1	$5.3x10^3$
Condensate 1	$3.0x10^7$
Wet Gas 1	$4.4x10^7$
Dry Gas 1(λ=1))	$7.3x10^7$
Dry Gas 1(λ=0.55)	$7.3x10^7$
Water	$1.3x10^3$
Dry Gas 2 (λ=1)	$2.26x10^8$
Dry Gas 2 (λ=0.55)	$2.26x10^8$
Wet Gas 2 (λ=1)	$1.97x10^8$
Wet Gas 2 (λ=0.75)	$1.97x10^8$
Condensate 2 (λ=1)	$7.26x10^7$
Condensate2 (λ=0.75)	$7.26x10^7$
Volatile Oil 3	$1.21x10^4$

4.2 Case Studies for Flow below the Saturation Pressure

Table 4.13 presents the compiled results for the t_D multiplier (viscosity-compressibility multiplier) as well as the q_D multiplier against the C_{7+} fractions for flow in shale wells operating below the corresponding saturation pressures.

Table 4.3—t_D multipliers of fluids below saturation pressure

Fluid Composition	t_D Multiplier ($x10^{-4}$)	q_D Multiplier	C_{7+} Mole Fraction
Dry Gas 1 (λ=0.55)	2.0	1/10000	0
Dry Gas 1 (λ=1)	3.5	1/10000	0
Wet Gas 1 (λ=0.55)	3.5	1/100000	9.2
Wet Gas 1(λ=1)	6.2	1/100000	9.2
Condensate 1 (λ=0.75)	1.5	1/20000	10
Condensate 1(λ=1)	2.2	1/20000	
Volatile Oil 2	1.2	1.5	24
Volatile Oil 1	2.7	1	16.8
Dry Gas 2 (λ=1)	7.0	1/50000	0
Dry Gas 2 (λ=0.55)	2.0	1/25000	0
Wet Gas 2 (λ=1)	9.0	1/60000	0.8
Wet Gas 2 (λ=0.75)	5.0	1/40000	0.8
Condensate 2 (λ=1)	7.0	1/16000	11.8
Condensate 2 (λ=0.75)	4.5	1/16000	11.8
Volatile Oil 3	8.0	2.5	21.8

Table 4.4 provides a list of values of predicted EUR for the wells with the given fluid compositions. The term AUC refers to Area under the Curve.

Table 4.4—Mathematical simulator calculations of the rate integral termed area under the matched curve (AUC) for q vs t for below saturation pressure.

Fluid Composition	EUR AUC q vs t
Volatile Oil 1	5.33×10^3
Volatile Oil 2	2.20×10^4
Condensate 1	2.95×10^7
Wet Gas1 (λ=0.55)	4.40×10^7
Dry Gas 1 (λ=1)	4.02×10^8
Dry Gas 2 (λ=1)	2.3×10^8
Dry Gas 2 (λ=0.55)	2.3×10^8
Wet Gas 2 (λ=1)	4.3×10^8
Wet Gas 2 (λ=0.55)	4.3×10^8
Condensate 2 (λ=1)	2.4×10^8
Condensate 2 (λ=0.75)	2.5×10^8
Volatile Oil 3	2.8×10^4

4.3 t_D Multiplier Correlation

The previous data illustrated that it is possible to extend the use of Carter (1985) type curves to more complex fluids for flow both above and below their respective saturation pressures. The workflow depends on identifying an appropriate viscosity-compressibility product that is valid over the entire life of the well. In this section, I explore the relationship between the viscosity-compressibility product and the fluid C_{7+} fractions.

Figure 4.1 shows the data plotted for all fluid types for the results presented in Chapter 3 for flow above the saturation pressure while Figure 4.2 shows the same results for flow below the fluid saturation pressure.

In Figure 4.1, although the results appear scattered, there appears to be a linear increase in the viscosity-compressibility multiplier as the C_{7+} fraction increases. For flow below the saturation pressure, the viscosity-compressibility multiplier decreases marginally as the C_{7+} fraction increases.

In either case, it is not apparent that a correlation between the viscosity-compressibility multiplier and the C_{7+} fraction can be obtained through qualitative analysis, the linear trends described in Figures 4.1 and 4.2 may be used.

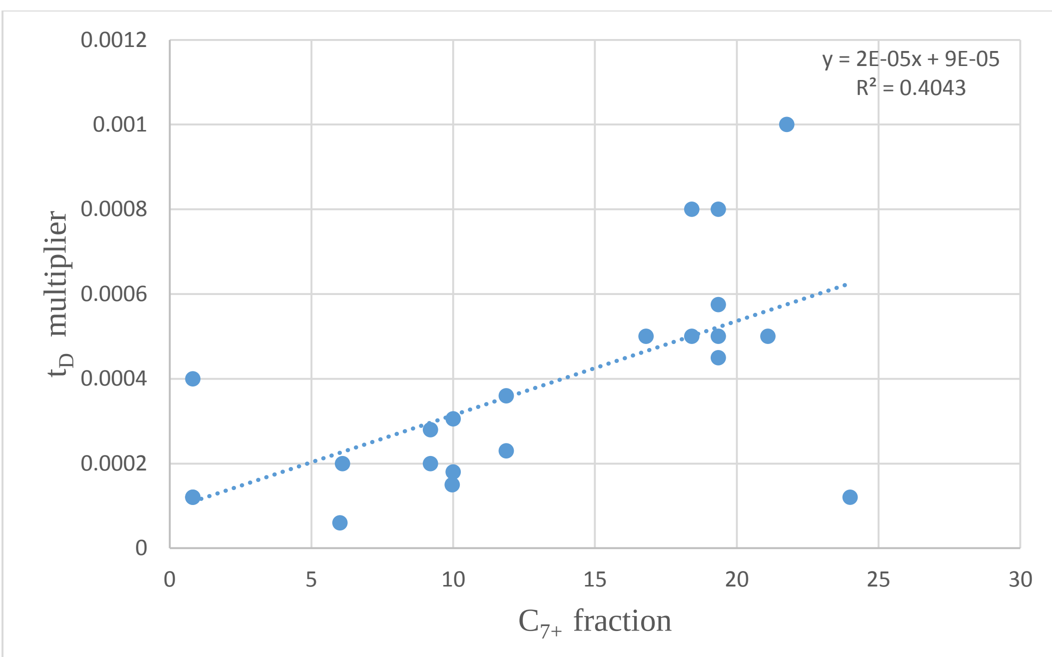

Figure 4.1—Graph of t_D multiplier vs C_{7+} fraction of fluid models above saturation pressure with a linear trend line.

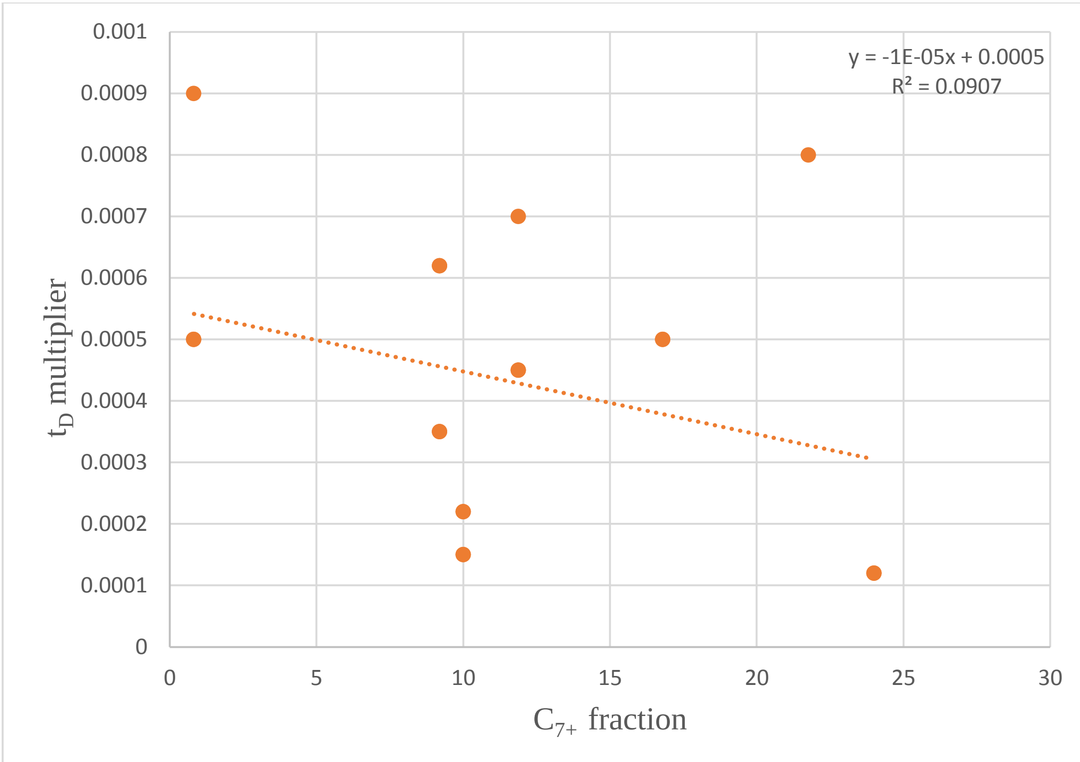

Figure 4.2—Graph of t_D multiplier vs C_{7+} fraction of fluid models below saturation pressure with a linear trend line.

4.4 EUR of Case Studies Above and Below Saturation Pressure

In this section, EUR values obtained from the type curve match are compared to the reservoir simulator output and present the percentage error in the type curve estimates. Tables 4.4 and 4.5 show these results for flow above and below the saturation pressures respectively. The tables illustrate that although a correlation with the C_{7+} fraction is somewhat challenging; the viscosity-compressibility multiplier allows us to obtain relatively accurate EUR values.

Table 4.5—Calculated EUR using type curves for models above saturation pressure

Fluid Composition	Cumulative Production	EUR Type Curve	% Error
Volatile oil 1	5.2Mbbl	4.96 Mbbl	4.8%
Condensate 1(λ=0.75)	29.5MMscf	26.8MMscf	10.0%
Wet Gas 1	41.8MMscf	46.4 MMscf	9.9%
Volatile oil 2	21.4Mbbl	26.1 Mbbl	21.0%
Dry Gas 1 (λ=1)	72 MMscf	70 MMscf	2.9%
Dry Gas 1 (λ=0.55)	72 MMscf	61 MMscf	18%
Water	1.26 Mbbl	1.2Mbbl	7.7%
Volatile 2	11.7 Mbbl	11.9 Mbbl	2.2%
Condensate2 (λ=1)	70 MMscf	73.5 MMscf	5.3%
Condensate2(λ=0.75)	70 MMscf	84 MMscf	17.0%
Wet Gas 2 (λ=1)	190 MMSCF	148 MMscf	28.0%
Wet Gas 2 (λ=0.75)	190 MMscf	189.6 MMscf	0.2%
Dry Gas 2 (λ=1)	219 MMscf	267 MMscf	18.0%
Dry Gas 2 (λ=0.55)	219 MMscf	267 MMscf	18.0%

Table 4.6−Calculated EUR using type curves for models below saturation pressure

Fluid Composition	Simulator EUR	EUR Type Curve	% Error
Volatile oil 2	46.5Mbbl	44.8Mbbl	3.8%
Volatile oil 1	5.3Mbbl	5.0Mbbl	5.5%
Condensate 1	29.6 MMscf	28.5MMscf	3.7%
Wet Gas 1	44 MMscf	42.7MMscf	3.0%
Dry Gas 1	402 MMscf	384MMscf	4.7%
Dry Gas 2 (λ=1)	219MMscf	267 MMscf	17.0%
Dry Gas 2 (λ=0.55)	219MMscf	259MMscf	15.0%
Wet Gas 2 (λ=1)	422MMscf	509 MMscf	17.0%
Wet Gas 2 (λ=0.55)	422MMscf	503 MMscf	16.0%
Condensate 2 (λ=1)	248MMscf	266 MMscf	6.8%
Condensate2(λ=0.75)	248MMscf	265 MMscf	6.4%
Volatile oil 3 (λ=1)	27.8Mbbl	22.5 Mbbl	23.5%

Chapter Five: Conclusions and Recommendations

In this thesis, I present an approach to extend the use of the Carter (1985) type curves for complex fluid types for flow both above and below the saturation pressures. The goal was to determine an effective viscosity-compressibility product that is valid for the entire life of the well and are correlated to the fluid C_{7+} fractions. The following are the conclusions from this work:

- The viscosity-compressibility product multipliers show a strong relationship with the fluid C_{7+} fraction, but obtaining a correlation is challenging because of the high degree of scatter in the data.
- The EUR calculations using the modified viscosity-compressibility product is fairly reliable and for the test cases considered, has a reasonable agreement with the accurate values.

Recommendations

- In this work, I did not consider the role of multiphase flow on the phase permeabilities over the life of the well. The intent was to focus on the viscosity-compressibility product. It is possible that the quality of the correlation shown in Chapter 4 will be improved if the fluid phase permeabilities are considered.
- The use of pore proximity correction is not used in this research because the reservoir simulators currently do not have this application available.

References

Ahmadi, H.A.A., Almarzooq, A.M., and Wattenbarger, R.A. 2010. Application of Linear Flow Analysis to Shale Gas Wells - Field Cases. Presented at the SPE Unconventional Gas Conference, Pittsburgh, Pennsylvania, USA, 23-25 February. SPE 130370-MS.
http://dx.doi.org/10.2118/130370-MS

Ali, M. T., and El-Banbi, A. H. 2015. EOS Tuning – Comparison between Several Valid Approaches and New Recommendations. Presented at SPE North Africa Technical Conference and Exhibition, Cairo, Egypt, 14-16 September**.**SPE-175877-MS.
http://dx.doi.org/10.2118/175877-MS

Arps, J. J.1945. Analysis of Decline Curves. Transactions of the AIME, **160** (01): 228-247.SPE-945228-G.
http://dx.doi.org/10.2118/945228-G.

Behrenbruch, P., and Goda, H. M.2006. Two-Phase Relative Permeability Prediction: A Comparison of the Modified Brooks-Corey Methodology with a New Carman-Kozeny Based Flow Formulation. Presented at SPE Asia Pacific Oil & Gas Conference and Exhibition, 11-13 September, Adelaide, Australia.SPE 101150-MS. http://dx.doi:10.2118/101150-MS.

Carslaw, H. S. and Jaeger, J. C.1921.*Some Two-Dimensional Problems. In Conduction of Heat with Circular Symmetry*. Proc., London Mathematical Society (2), Vol S2-46, Issue 1,361-365.

Carslaw, H. S and Jaeger, 1. C.1941. *Operational Methods in Applied Mathematics*, first edition. Oxford Univ. Press.

Carslaw, H. S., Jaeger, J. C., and Feshbach, H.1962. *Conduction of Heat in solids*. Physics Today, 15(11), 74-76.

Carter, R. D.1962.Solutions of Unsteady-State Radial Gas Flow. Journal of Petroleum Technology (5) 549-554.SPE 108-PA.
http://dx.doi.org/10.2118/108-PA.

Carter, R. D.1981. Characteristic Behavior of Finite Radial and Linear Gas Flow Systems - Constant Terminal Pressure Case. Presented at SPE/DOE Low Permeability Gas Reservoirs Symposium, 27-29 May, Denver, Colorado. SPE 9887-MS http://dx.doi.org/10.2118/9887-MS.

Carter, R. D.1985. Type Curves for Finite Radial and Linear Gas-Flow Systems: Constant Terminal Pressure Case. SPE Journal. SPE 12917 PA. http://dx.doi:10.2118/12917-PA.

Chaudhary, A. S., Ehlig-Economides, C. A., & Wattenbarger, R. A.2011. Shale Oil Production Performance from a Stimulated Reservoir Volume. SPE Annual Technical Conference and Exhibition, 30 October-2 November, Denver, Colorado, USA. http://dx.doi:10.2118/147596-MS.

Chatas, A. T. and Malekfam, H.1970. The Estimation of Aquifer Properties from Reservoir Performance in Water-Drive Fields. Society of Petroleum Engineers. January 1. SPE 2970-MS. http://dx.doi:10.2118/2970-MS.

CMG 2016. http://www.cmgl.ca/software.

Earlougher, Robert C. 1977. *Advances in well test analysis*, second edition. Monograph series of Society of Petroleum Engineers of AIME, Chapter 5,264. Dallas, TX: Millet the Printer Inc.

Eclipse 2016, Schlumberger. https://www.software.slb.com/products/eclipse.

Fetkovich, M. J.1980. Decline Curve Analysis Using Type Curves. Journal of Petroleum Technology.1 June. SPE 4629-PA http://dx.doi:10.2118/4629-PA.

Fetkovich, M. J. 1980. Enlarged Type Curves Supporting Paper SPE 4629. Society of Petroleum Engineers Journal of Petroleum Technology **30** (06):1065-1077.SPE-9086-MS. (in press; posted June 1980). http://dx.doi:10.2118/9086-MS.

Fetkovich, M. J., Vienot, M. E., Bradley, M. D., & Kiesow, U. G.1987. Decline Curve Analysis Using Type Curves: Case Histories. Society of Petroleum Engineers Formation Evaluation Vol **2** (04): 637-656. SPE 13169-PA (in press; posted 1 December).
http://dx.doi:10.2118/13169-PA.

Fraim, M. L and Wattenbarger, R.A.1987.Gas Reservoir Decline-Curve Analysis Using Type Curves with Real Gas Pseudo pressure and Normalized Time. SPE Formation Evaluation 2 (04): 671-682. December. SPE 14238-PA.
http://dx.doi:10.2118/14238-PA.

Ilk, D., and Blasingame, T. A. 2013. Decline Curve Analysis for Unconventional Reservoir Systems-Variable Pressure Drop Case. SPE Unconventional Resources Conference Canada, 5-7 November, Calgary, Alberta, November 5-7. SPE 167253-MS.
http://dx.doi:10.2118/167253-MS.

Kabir, C. S., & Lake, L. W.2011. An Analytical Approach to Estimating EUR in Unconventional Reservoirs. Society of Petroleum Engineers. SPE 144311-MS.
http://dx doi: 10.2118/144311-MS.

Lee, W. John, and Robert A. Wattenbarger. 1996. Decline-Curve Analysis for Gas Wells. Gas reservoir engineering. Vol. 5. First Printing, Chapter 9-11, 214-271. Richardson, Texas. Society of Petroleum Engineers Inc.

Locke, C.D. and Sawyer, W.K.1975.Constant Pressure Injection Test in a Fractured Reservoir-History Match Using Numerical Simulation and Type Curve Analysis. Presented at the SPE Annual Technical Conference and Exhibition, Dallas, 28 Sept.-Oct. SPE-5594- MS.
http://dx doi: 10.2118/5594-MS.

MATLAB 2016.https://www.mathworks.com/products/matlab.html.

McCain, W.D.J. 1990. "*Properties of Petroleum Fluids"*, 2nd Edition. Chapter 5, 147-164. Pen well Books, Pen well Publishing Co. Tulsa, Oklahoma.

Moinfar, A., Erdle, J. C., and Patel, K. 2016. Comparison of Numerical vs Analytical Models for EUR Calculation and Optimization in Unconventional Reservoirs.

Presented at the SPE Low Perm Symposium, Denver, Colorado, USA. May 5. SPE 180209-MS. http://dx.doi:10.2118/180209-MS.

Moore, T.V., Schilthuis, R.J., and Hurst, W.1933.The Determination of Permeability from Field Data, Bull., API. May, 111, 4.

Okouma Mangha, V., Guillot, F., Sarfare, M., San, V., Ilk, D., & Blasingame, T. A. 2011. Estimated Ultimate Recovery (EUR) as a Function of Production Practices in the Haynesville Shale. Society of Petroleum Engineers. SPE 147623-MS. http://dx. doi:10.2118/147623-MS.

Pratikno, H., Rushing, J. A., & Blasingame, T. A.2003. Decline Curve Analysis Using Type Curves - Fractured Wells. Presented at the SPE Annual Technical Conference and Exhibition, Denver, Colorado, 5-8 October. SPE 84287. http://dx.doi:10.2118/84287-MS.

Raghavan, R., Scorer, D. T., and Miller, F. G.1972.An Investigation by Numerical Methods of the Effect of Pressure Dependent Rock and Fluid Properties on Well Flow Tests, 267-276.

Rodrigues, E. S., and Callard, J. G. 2012. Permeability and Completion Efficiency Determination from Production Data in the Haynesville, Eagle Ford and Avalon Shales. Presented at the SPE Annual Technical Conference and Exhibition, Denver,Colorado,21-24September.SPE-161335-MS. http://dx.doi:10.2118/161335-MS.

Samaniego V., Fernando, and Cinco L., Heber. 1980.Production Rate Decline in Pressure-Sensitive Reservoirs. Journal of Canadian Petroleum Technology **19** (03). July-September. JCPT 80-03-03 (in press; posted July 1980)
.

Sanni, M. O., and Gringarten, A. C. 2008. Well Test Analysis in Volatile Oil Reservoirs. Presented at the SPE Annual Technical Conference and Exhibition, Denver, Colorado, 21-24 September. SPE 116239-MS. http://dx.doi:10.2118/116239-MS.

Schenewerk, P. A., and Heath, B. 1989. A Case Study of Improved Recovery Options in a Volatile Oil Reservoir. Presented at the SPE Annual Technical Conference and Exhibition, San Antonio, Texas, 8-11 October. SPE 19837-MS. http://dx. doi:10.2118/19837-MS.

Schilthuis, R.J. "Active Oil and Reservoir Energy", Trans AIME (1936)118,33-52.

Spivey, J. P., Gatens, J. M., Semmelbeck, M. E., & Lee, W. J. 1992. Integral Type Curves for Advanced Decline Curve Analysis. Presented at the SPE Mid-Continent Gas Symposium, Amarillo, Texas, 13-14 April. SPE 24301-MS. http://dx.doi:10.2118/24301-MS.

Spivey, J. P., and McCain, W.D. 2013. Estimating Reservoir Composition for Gas Condensates and Volatile Oils from Field Data. Presented at the SPE Annual Technical Conference and Exhibition, New Orleans, Louisiana, 30 September-2 October. SPE 166414-MS. http://dx.doi:10.2118/166414-MS.

Swami, V., Settari, A., Sahai, R., Costello, D., & Mercer, A. (2017, February 15). A Novel Approach to History Matching and Optimization of Shale Completions and EUR - A Case Study of Eagle Ford Well. Presented at the SPE Unconventional Resources Conference, Calgary, Alberta, 15-16 February. SPE 185075-MS. http://dx.doi:10.2118/185075-MS.

Texas Rail Road Commission.2016. Production data.http://www.rrc.state.tx.us/oil-gas/research-and-statistics/production-data/

Rubin, B. 2010. Accurate Simulation of Non Darcy Flow in Stimulated Fractured Shale Reservoirs. Presented at the SPE Western Regional Meeting, Anaheim, California, 27-29 May. SPE 132093-MS. http://dx. doi:10.2118/132093-MS.

Van Everdingen, A. F., & Hurst, W. 1949. The Application of the Laplace Transformation to Flow Problems in Reservoirs. Society of Petroleum Engineers Journal of Petroleum Technology **1** (12): 305-324. December 1. SPE 949305-G. http://dx.doi:10.2118/949305-G.

Zhang, M., & Ayala, L.2014. Gas-Production-Data Analysis of Variable-Pressure-Drawdown/Variable-Rate Systems: A Density-Based Approach. Society of Petroleum Engineers Reservoir Evaluation and Engineering **17** (04): 520-529. November 1. SPE 172503-PA
http://dx.doi:10.2118/172503-PA.

Appendix A: Nomenclature

A = area of flow system in the plane normal to the direction of flow, sq. ft. [m^2]

b= reciprocal of decline-curve exponent

B_j = coefficient of the jth term

B_o= Formation volume factor, reservoir volume/surface volume

c_e = effective compressibility, psi^{-1} [kPa^{-1}]

$c_{g(p)}$ = gas compressibility, psi^{-1} [kPa^{-1}]

$\overline{c_g}$= area-averaged reservoir gas compressibility,1/psi

c_o = compressibility of oil, psi^{-1} [kPa^{-1}]

c_w= compressibility of water, psi^{-1} [kPa^{-1}]

c_t = total compressibility, psi -^{1} [kPa^{-1}]

$G_p(t)$ = cumulative gas production, m^3, MMscf

G_{DR}, G_{DL} = dimensionless cumulative production expressed as a fraction of the gas that would be recovered by reducing the average reservoir pressure from p_i to p_{wf}

$G_{(p)}$ = reservoir gas content corresponding to average reservoir pressure p, MMscf or MMscf [std. m^3]

D_i = initial decline rate, t=1day, t^{-1}

Δ = symbol used for change in value

e = natural logarithm base, 2.71828

G = gas in place at start of decline analysis, surface-measured

G_i = initial gas in place, surface-measured

G_p = cumulative gas production, surface-measured

h = pay thickness, ft. [m]

J_n = Bessel function of first kind of order n

k = effective permeability, md

L = length of linear system parallel to the direction of flow, ft. [m]

L_{xe} = reservoir half-length, ft. [m]

L_{xf}= fracture half-length, ft. [m]

m (p) = real gas pseudo pressure of real gas flow potential psi^2/cp [(kPa)^2/(Pa. s)]

m (p_i) = pseudo pressure evaluated at initial reservoir pressure

m (p_{wf}) = pseudo pressure evaluated at wellbore pressure

p = pressure, psia [kPa]

p_i = initial reservoir pressure, psia [kPa]

p_{wf} = bottom hole flowing pressure, psia [kPa]

p' = pressure variable of integration, psia [kPa]

q_g = gas production rate, MMscf/d [std. m^3/d]

q_{gsc} =gas flow rate at standard conditions, scf/day

q_D = dimensionless rate used in the type curves, defined by Eq. A-18

q_{DR} = dimensionless time

q_o = oil production rate, STB/d [stock-tank m^3/d]

r_e = external radius of type curve reservoir region, ft. [m]

r_w = internal radius of type curve reservoir region, ft. [m]

R = radius ratio r_e/r_w.

S_w = water saturation, fraction

t = time, days [d]

t_D = dimensionless time used in the type curves

t_{dD}= decline-curve dimensionless time

t_{DL} = dimensionless time as defined by 1

t_{DR} = dimensionless time defined

T = reservoir temperature, R or [K]

μ_g= viscosity of gas, cp

$\overline{\mu_g}$ = space averaged reservoir gas viscosity, cp

Y_n = Bessel function of second kind of order n

$z_{(p)}$ = gas deviation (or super compressibility) factor, dimensionless

α_j = time coefficient in the j_{th} term in Bessel equations

η= type curve parameter characterizing effect of radius ratio R, dimensionless

q_{Dd} = dimensionless cumulative production

G_{DR} = recoverable gas to the point where average reservoir pressure has equalized with the constant BHFP, L^3, MMscf

λ= type-curve parameter used to characterize gas well drawdown, dimensionless

μ= gas viscosity, cp [Pa. s]

$\mu_g c_g$ = mean value of viscosity/compressibility product over the pressure interval p_i to p_{wf}, cp/psi [Pa. s/kPa]

σ = fraction of 2π radians defining the concentric ring sector constituting the type curve approximation to the reservoir shape, dimensionless

Φ= hydrocarbon porosity (for a gas reservoir, usually porosity times [1-s_w]), fraction